A megaprotein-based molecular bridge critical for lipid trafficking and cold resilience

Changnan Wang[1, 2, †], Bingying Wang[1, †], Taruna Pandey[1], Yong Long[3], Jianxiu Zhang[4], Fiona Oh[1], Jessica Sima[1], Ruyin Guo[1], Yun Liu[7], Chao Zhang[2], Shaeri Mukherjee[5], Michael Bassik[6], Weichun Lin[7], Huichao Deng[8], Goncalo Vale[9], Jeffrey McDonald[9], Kang Shen[8], Dengke K. Ma[1, 10, *]

[1]Cardiovascular Research Institute and Department of Physiology, University of California San Francisco, San Francisco, USA

[2]Shanghai Institute of Precision Medicine, Shanghai Ninth People's Hospital, Shanghai Jiao Tong University School of Medicine, Shanghai, China

[3]State Key Laboratory of Freshwater Ecology and Biotechnology, Institute of Hydrobiology, Chinese Academy of Sciences, Wuhan, China.

[4]Department of Molecular and Cellular Physiology, Stanford University, Stanford, CA, USA

[5]Department of Microbiology and Immunology, University of California, San Francisco, San Francisco, CA 94143, USA

[6]Department of Genetics, Stanford University School of Medicine, Stanford, CA 94305, USA

[7]Department of Neuroscience, University of Texas Southwestern Medical Center, Texas, USA

[8]Department of Biology, Stanford University, Stanford, CA 94305, USA

[9]Center for Human Nutrition, University of Texas Southwestern Medical Center, Dallas, USA.

[10]Innovative Genomics Institute, University of California, Berkeley, CA 94720, USA.

†These authors contributed equally to this work, * Correspondence: Dengke.Ma@ucsf.edu

Abstract

Cells adapt to cold by increasing levels of unsaturated phospholipids and membrane fluidity through homeostatic mechanisms conserved in nearly all forms of life. As most eukaryotic enzymes for lipid synthesis and desaturation localize on endoplasmic reticulum (ER) membranes, it remains unknown how ER-resident lipids rapidly distribute to plasma membranes (PM). Here we report an exceptionally large and evolutionarily conserved protein LPD-3 in *C. elegans* that plays critical roles in lipid trafficking and cold resilience. We identified *lpd-3* mutants in a mutagenesis screen for genetic suppressors of the lipid desaturase FAT-7, and found that the 452 kDa megaprotein LPD-3 bridges ER and PM, consisting of a structurally predicted hydrophobic tunnel for lipid trafficking. Loss of LPD-3 caused abnormal cellular distribution of phospholipids, diminished FAT-7 abundance, and organismic vulnerability to cold. These phenotypic defects of *lpd-3* mutants were rescued by Lecithin comprising unsaturated phospholipids. Importantly, we found that deficient *lpd-3* homologues in Zebrafish and mammalian cells led to defects similar to those observed in *C. elegans*. As mutations in *KIAA1109/BLTP1*, the human orthologue of *lpd-3*, cause Alkuraya-Kucinskas syndrome, we propose that the LPD-3 family proteins may serve as evolutionarily conserved "highway bridges" critical for ER-associated non-vesicular trafficking of lipids and resilience to cold stress in eukaryotic cells.

Introduction

Homeoviscous adaptation (HVA) refers to the ability of cells to adjust membrane viscosity by changing cell membrane lipid compositions and unsaturation in response to environmental temperature shifts[1–3]. For example, exposure to cold temperature in bacteria rigidifies cell membrane, triggering HVA to maintain membrane fluidity within a normal range to ensure proper activity of membrane proteins[2]. Besides bacteria, HVA has been observed in many eukaryotic organisms as an evolutionarily conserved mechanism that enables adaptation to changes in environmental temperature. In both bacteria and the multicellular model organism *C. elegans*, HVA involves temperature-triggered transcriptional regulation of genes encoding lipid desaturases. While heat down-regulates a fatty acid desaturase-encoding gene *fat-7* through *acdh-11*, cold up-regulates *fat-7* through the membrane fluidity sensor PAQR-2 and transcriptional regulators in *C. elegans*[3–6]. Temperature-regulated FAT-7 catalyzes chemical C=C double bond formation in fatty acyl chains leading to membrane lipid desaturation and increased membrane fluidity. HVA through such regulation of lipid desaturases facilitates cellular adaptation to, and orgasmic survival against, environmental temperature stresses[1–3].

In eukaryotes, lipid biosynthetic enzymes and lipid desaturases, including FAT-7, are located at the endoplasmic reticulum (ER). The newly synthesized and unsaturated lipids can distribute to other cellular organelles by both well-characterized vesicular transport pathways and less well-understood non-vesicular transport mechanisms[7,8]. Earlier studies indicate that inhibition of vesicular transport pathways does not substantially decrease transfer of phospholipids, including phosphatidylcholine (PC) and phosphoatidylethanolamine (PE), from ER to plasma membranes (PM)[9,10]. More recent studies suggest that non-vesicular lipid trafficking among various intracellular organelles, including ER, lysosomes and mitochondria, occurs through a conserved

family of RBG domain-containing VPS13-like lipid transporters[11–16]. However, compared to the vesicular lipid transport pathways, mechanisms of action, physiological regulation and organismic functions of non-vesicular lipid transporters remain still largely unknown.

We performed a mutagenesis screen for genetic suppressors of FAT-7 in *C. elegans* and identified *lpd-3*, which encodes a 452 k.D. megaprotein bridging the ER and PM. AlphaFold2-assisted structural prediction reveals an elongated hydrophobic tunnel in LPD-3 suited for lipid trafficking. We show that LPD-3 is critical for *fat-7* expression, normal distribution of phospholipids at the PM, and organismic resilience to severe cold stress. Mutations in *KIAA1109*/*BLTP1*, the human orthologue of *lpd-3*, cause an autosomal recessive disorder, Alkuraya-Kucinsk syndrome[17–20]. We found that decreased expression of *lpd-3* homologues in Zebrafish and mammalian cells elicited similar phenotypes as in *C. elegans*. Our results suggest evolutionarily conserved roles of the LPD-3 family proteins as megaprotein-based molecular bridges in non-vesicular trafficking of lipids and stress resilience to cold temperature.

Results

Genetic screens identify LPD-3 as a key regulator of FAT-7

We have previously discovered components of a genetic pathway in *C. elegans* that maintains cell membrane fluidity by regulating lipid desaturation via the fatty acid desaturase FAT-7 in response to temperature shifts[3]. Loss-of-function mutations in the gene *acdh-11* cause constitutive FAT-7 up-regulation. In forward genetic screens to isolate mutants with *acdh-11*-like constitutive expression of *fat-7*::GFP, we identified several alleles of *acdh-11* and two additional genes, *cka-1* and *sams-1* (Fig. 1a, Extended Data Fig. 1a, b), which are involved in

cellular phosphatidylcholine biosynthesis[21–23]. *acdh-11*, *cka-1* and *sams-1* encode negative regulators of *fat-7*. To identify positive regulators of *fat-7*, we performed *acdh-11* suppressor screens for mutants with diminished *fat-7*::GFP (Fig. 1a). Unlike loss-of-function mutants of known positive regulators (e.g. *nhr-49/80* or *sbp-1* with complete loss of *fat-7*::GFP signals)[24–27], a rare *acdh-11* suppressor mutant *dma544* exhibits diminished *fat-7*::GFP in the anterior intestine and decreased (but still visible) *fat-7*::GFP in the posterior intestine (Extended Data Fig. 2a, b). By single nucleotide polymorphisms-based genetic mapping and whole-genome sequencing, we identified *dma544* as a missense transition mutation of the gene *lpd-3*. RNAi against *lpd-3*, an independently derived deletion mutation or another *acdh-11* suppressor *dma533* recapitulated both *fat-7*::GFP suppression and the morphological pale phenotype of *dma544* (Fig. 1b, c). RNAi against *lpd-3* also suppressed *fat-7*::GFP in the *cka-1* or *sams-1* mutants (Extended Data Fig. 1c).

LPD-3-regulated transcriptome and FAT-7-related phenotypes

To better understand functions of LPD-3, we assessed how *lpd-3* mutations alone might impact gene expression changes and *fat-7*-related phenotypes without *acdh-11* mutations. In the wild type, *fat-7*::GFP was increased upon exposure to a cold temperature at 15 ^{o}C, yet such increase was abolished in *lpd-3* mutants (Extended Data Fig. 2c). The baseline expression of *fat-7*::GFP at 20 ^{o}C was also abolished in *lpd-3* mutants, including that in the posterior intestine (Fig. 1c). We performed RNA sequencing (RNAseq) to compare transcriptomes of wild type versus *lpd-3* mutants cultivated at 20 ^{o}C. After differential expression analyses of triplicate samples, we identified 6251 genes that are significantly up- or down-regulated in *lpd-3* mutants (Fig. 1d). As expected, *fat-7* was one of the most highly down-regulated genes ($\log_2$fold change = -5.05, adjusted p value = 2.54E-13), while expression of its upstream regulators including *cka-1*, *sams-1* or *acdh-11* remained largely unchanged (Fig. 1e, Extended Data Table 1). Among the genes

that were significantly up-regulated (adjusted p value > 0.05), 234 genes were also up-regulated by exposure to 4 ºC cold-warming stress[28], including the previously validated cold-inducible gene *asp-17* that we confirmed to increase dramatically in *lpd-3* mutants without cold exposure (Extended Data Fig. 3c). We used WormExp[29] to compare these 234 genes to expression data from all previously characterized mutant animals and found they were significantly similar (*P* = 1.7e-107) to the gene set regulated by RNAi against *sbp-1* (Extended Data Fig. 3d)[30]. RNAi against *lpd-3* or *sbp-1* has previously been shown to induce the morphological pale and lipid depletion phenotypes[25,31–33]. We confirmed such phenotype in *lpd-3(dma544)* mutants (Fig. 1c, f) and further showed that deletion of LPD-3 caused markedly fewer and smaller lipid droplets using an established lipid droplet marker DHS-3::GFP[34] (Extended Data Fig. 4). We made similar observation in animals with RNAi against *sbp-1*, which encodes a master regulator of lipogenesis and *fat-7* expression for unsaturated lipid accumulation in *C. elegans*[24,25,35,36] (Extended Data Fig. 4). These results identify transcriptomic gene expression changes as well as *fat-7*-related lipid and morphological phenotypes in *lpd-3* mutants.

Structural features and cellular localizations of LPD-3

We next examined structural features of LPD-3 that may provide insights into its molecular function. LPD-3 is an exceptionally large protein, consisting of predicted 4,018 amino acid residues of 452 kDa molecular weight. We sought to obtain a predicted LPD-3 structure by the machine-learning-based AlphaFold2 program[37]. As the program is limited to polypeptides smaller than 2,000 amino acids, we segmented the full-length LPD-3 sequence into eight overlapping parts that were separately predicted and then rejoined to generate a full-length structure (Fig. 2a). The yielded full-length structure reveals an approximately 30 nm-long rod-like shape consisting of twisted β-sheets that form a striking tubular cavity and internal

hydrophobic tunnel extending along its entire length (Fig. 2a, b). The *dma544* mutation (G200E) disrupts a highly conserved glycine residue lining up the internal tubular wall while the resulting G200E glutamic acid residue of LPD-3 is predicted to partially block the tunnel entry (Fig. 2c). The N-terminal sequence of LPD-3 forms a putatively hydrophobic transmembrane helix while its C-terminal sequence harbors an amphiphilic patch and a polybasic cluster (KxKK motif that binds to PIP2/PIP3) indicative of association with the cytosolic side of lipid membranes[38] (Fig. 2d). These structural features of LPD-3 are reminiscent of the recently described VPS13 family transporters that mediate non-vesicular lipid trafficking across organelle membranes[11–13,16], although these separate families of proteins lack apparent protein sequence similarity.

To determine the subcellular localization of LPD-3, we constructed transgenic reporters for both N- and C-termini of LPD-3. A mCherry-tagged N-terminal LPD-3 translational reporter showed prominently discrete intracellular signals in the intestine (Fig. 2e). We crossed this N-terminal reporter into established *C. elegans* strains expressing bright fluorescent GFP directed to various intracellular organelles including Golgi (mans::GFP), mitochondria (MAI-2::GFP), peroxisome (GFP::DAF-22), lysosome (LMP-1::GFP), endosome (RAB-7::GFP) and ER membranes (GFP::C34B2.10::SP12). We found that the N-terminal LPD-3::mCherry was localized exclusively at the ER membrane (Fig. 2e). By contrast, a mCherry-tagged C-terminal LPD-3 translational reporter displayed both intracellular and plasma membrane (PM) signals in the intestine (Fig. 2f). We found that the PM signal of mCherry-tagged C-terminal LPD-3 was co-localized with Akt-PH::GFP, an established reporter that binds to the phospholipid PIP2/PIP3 of the inner leaflet of PM[39] (Fig. 2f). We also used CRISPR/Cas9 to generate knock-in of seven copies of GFP at the C-terminus of endogenous LPD-3 and reconstitution with GFP1-10 allowed us to observe weak but detectable fluorescent reporter signals in the intestine and hypoderm.

Although the intestinal autofluorescence precluded unambiguous identification of weak LPD-3::GFP signals in the intestine, we found that endogenous LPD-3::GFP in the hypoderm appears to localize in discrete domains along the boundary of mScarlet::ATLN-1 (a tubular ER membrane protein that helps maintain the non-uniform distribution of ER–plasma membrane contacts[40]) (Fig. 2g), consistent with the probable localization of LPD-3 at ER-PM membrane contact sites that mediate lipid trafficking and integrate phospholipid regulation[41–43].

Essential roles of LPD-3 in ER-to-PM lipid trafficking and SBP-1 regulation

The structural features and cellular localizations of LPD-3 indicate an ER-to-PM bridge-like tunnel with plausible roles in mediating non-vesicular ER-to-PM trafficking of lipids. Next, we conducted a series of functional experiments and phenotypic analyses to test this idea.

First, we examined how LPD-3 may impact phospholipid distribution in the cell. Phospholipids, including phosphatidylcholine (PC), phosphatidylserine (PS), phosphatidylethanolamine (PE) and phosphatidylinositol (PI), are newly synthesized at the ER and transported to cytoplasmic membranes through both vesicular and non-vesicular mechanisms[7,8]. Since probes for live monitoring of most phospholipid distribution are unavailable in *C. elegans*, we took advantage of the genetically encoded reporter Akt-PH::GFP, which binds to the phospholipid PIP2 (4,5-bisphosphate) and PIP3 (3,4,5-phosphate), to assess the intracellular distribution and abundance of PIP2/PIP3 species[39]. We found that wild-type animals exhibited AKT-PH::GFP fluorescence enriched along the apical membrane of the intestine (Fig. 3a). By contrast, when crossed into *lpd-3* mutants, this same reporter at the same developmental stage (24 or 48 hrs after L4) showed attenuated overall fluorescence without apparent apical enrichment in the intestine, and more dispersed intracellular distribution compared to that in wild type (Fig. 3a). We also noticed that transgenic expression of mCherry-tagged C-terminal LPD-3 reduced the apical enrichment of

AKT-PH::GFP, indicating competition of both reporters for the same substrate (Fig. 2f). As PM-localized PIP2/PIP3 is associated with and often stimulates actin polymerization, we found that a filamentary actin reporter *act-5*::GFP[44] also displayed strikingly reduced abundance and apical localization in *lpd-3* mutants (Fig. 3b). These results reveal striking defects of PIP2/PIP3-binding reporter distribution in LPD-3-deficient intestinal cells and support the notion that LPD-3 normally promotes enrichment of phospholipids, at least certain PI species, at the PM.

Second, we examined how LPD-3 may impact functional consequences of loss of SAMS-1. The S-adenosyl methionine synthetase SAMS-1 is critical for the biosynthesis of phosphatidylcholine in *C. elegans*, decreased abundance of which on ER membranes activates ER stress response and expression of lipogenic genes including *fat-7* via SBP-1 regulation[21,45]. We found that *fat-7*::GFP was strongly activated by RNAi against *sams-1* in wild type but not in *lpd-3* mutants (Fig. 3c, d). We made similar observation on *hsp-4*p::GFP, an established reporter for ER stress response (Fig. 3e). These results indicate that LPD-3 antagonizes effects of SAMS-1 in PC accumulation at ER membranes, again supporting a physiological role of LPD-3 in facilitating the ER-to-PM trafficking of phospholipids, which reduces PC accumulation in ER membranes.

Third, we examined how LPD-3 may impact the nuclear abundance of SBP-1, a master regulator of lipogenesis and *fat-7*. The *C. elegans* SREBP homolog SBP-1 promotes lipogenesis and transcriptionally activates *fat-7* expression by translocating from ER membranes to nucleus [21,24,25]. We found that the abundance of nuclear SBP-1::GFP was markedly decreased by RNAi against *lpd-3* (Fig. 3f). By contrast, a transcriptional *sbp-1*p::GFP reporter was not apparently affected by *lpd-3* RNAi (Fig. 3f). These results indicate that LPD-3 promotes *fat-7* expression likely through post-transcriptional regulation of SBP-1. Since low PC levels in ER membranes

trigger SBP-1 nuclear translocation, these data are consistent with the notion that LPD-3 decreases PC levels in ER membranes by promoting ER-to-PM phospholipid trafficking.

Fourth, we examined how LPD-3 may impact cellular membrane integrity. Phospholipids with proper compositions of saturated and unsaturated fatty acyl chains are critical for the maintenance of membrane fluidity and integrity. Using a fluorescein-based SMURF assay to measure membrane permeability[46], we found that *lpd-3* mutants accumulated markedly higher levels of fluorescein in the intestine, and to a lesser extent in amphid sensory neurons, compared to wild type (Fig. 3h, i). These results suggest that loss of LPD-3 may compromise intestinal PM integrity. As insufficient fatty acyl unsaturation of phospholipids causes membrane leakiness via formation of domains with high-order phases that lack plasticity[47], we predict that loss of LPD-3 may lead to retention of excessively unsaturated phospholipids in ER membranes. Indeed, we found that excessive lipid saturation in ER membranes by RNAi against *mdt-15* activated ER stress response[45] in wild type but not *lpd-3* mutants (Extended Data Fig. 5a). Despite increased PM leakiness resulting from reduced unsaturated lipids, the intestinal PM morphology and PM-targeted trafficking of proteins with GFP prenylation reporters appeared largely normal in *lpd-3* mutants (Extended Data Fig. 5b), suggesting specific roles of LPD-3 in lipid trafficking.

Together, these results support that LPD-3 promotes ER-to-PM trafficking of phospholipids, and by doing so, to regulate SBP-1 nuclear abundance and expression of the *fat-7* gene.

Organismic phenotype and phospholipid/Lecithin rescue of *C. elegans lpd-3* mutants

To determine the physiological role of LPD-3 at the organismic level, we characterized *lpd-3* mutant phenotypes in development and adult resilience to cold exposure. Compared with wild type, *lpd-3* mutants show developmental delay, reaching to the larval L4 stage more slowly (Fig.

4a). In adult stages, *lpd-3* mutants are strikingly sensitive to both cold shock (4 ^{o}C for 20 hrs) and short-term freezing shock (-20 ^{o}C for 25 min) (Fig. 4b, Extended Data Fig. 6b). As *lpd-3* mutants showed probable defective ER-to-PM trafficking of phospholipid, we sought to rescue such organismic phenotypes of *lpd-3* mutants by supplementation of phospholipids from various sources and individual constituents of phospholipids, including choline, serine, ethanolamine and fatty acids (unsaturated oleic or saturated stearic acids). We found that phospholipids (from soy or egg yolks) or Lecithin (predominantly unsaturated PC-type glycerophospholipids), but not other compounds tested, fully rescued the developmental delay of *lpd-3* mutants (Fig. 4a, Extended Data Fig. 6a). Lecithin also rescued adult survival to cold exposure in a dose-dependent manner (Fig. 4c). Additional defects of *lpd-3* mutants in fecundity, cold or freezing tolerance, locomotory behavior, and intestinal membrane integrity or permeability were also rescued by Lecithin (Fig. 4e, Extended Data Fig. 6b-d). These data further support the functional role of LPD-3 in ER-to-PM phospholipid trafficking (Fig. 4f) and demonstrate a compelling pharmacological means by using Lecithin compounds to rescue defects in *lpd-3* mutants.

Conserved roles of LPD-3 family proteins in phospholipid trafficking and cold resilience

LPD-3 is the sole *C. elegans* orthologue of a highly evolutionarily conserved protein family including Tweek (*Drosophila*), Kiaa1109 (Zebrafish and mice) and KIAA1109 (Humans), recently renamed as BLTP1 (Extended Data Fig. 7a). To assess whether roles of LPD-3 in *C. elegans* are likely evolutionarily conserved in other organisms, we evaluated the consequences of loss of *lpd-3* orthologues in either mammalian cells or Zebrafish. We derived and cultured mouse embryonic fibroblast (MEF) cells from *Kiaa1109*-deficient mouse embryos[48]. Transfection with AKT-PH::GFP reporters showed that PIP2/PIP3 phospholipids as bound by AKT-PH::GFP were enriched at ruffling membranes of cell periphery in wild-type but not knock-out (KO) MEFs

(Fig. 5a). *Kiaa1109* KO MEFs also exhibited higher sensitivity to cold stress, and this defect was rescued by supplementation with Lecithin (Fig. 5b). We also used a click chemistry-based method[49] to image phospholipids based on metabolic incorporation of the choline analog propargylcholine into phospholipids (Fig. 5c). We found that both *Kiaa1109* KO MEFs and *lpd-3* mutant *C. elegans* exhibited striking reduction of fluorophore-conjugated propargylcholine signals at the PM (Fig. 5d, e, f). In HEK293 human cell lines, we co-expressed two plasmids encoding AKT-PH::GFP and shRNA against *KIAA1109* and found that knockdown of *KIAA1109* led to reduced PM localization of AKT-PH::GFP (Extended Data Fig. 7b), as in MEFs and *C. elegans*. In addition, CRISPR/Cas9-mediated KO of *KIAA1109* in U937 cells also markedly increased cell death after 4 ^{o}C cold stress (Extended Data Fig. 7c). In Zebrafish, we used morpholino (MO) to knockdown *kiaa1109* and found that *kiaa1109* MO caused curved body and head defects as reported[18] (Extended Data Fig. 7d, e). Using a cold sensitivity assay[50], we found that knockdown of *kiaa1109* led to striking reduction of fish survival against cold stress (Extended Data Fig. 7f, g). Unlike *C. elegans*, Zebrafish embryos did not readily uptake exogenous lipids provided in their diets, thus precluding us from testing Lecithin effects in Zebrafish models. Nonetheless, the convergent phenotypes of phospholipid reporters, metabolic labeling and cold tolerance we have observed in *C. elegans*, Zebrafish, mouse and human cells strongly support the evolutionarily conserved roles of LPD-3 family proteins in promoting cellular phospholipid trafficking at membrane contact sites of ER and resilience to cold stress.

Discussion

Based on our integrated genetic, protein structural, cell biological and organismic phenotypic analyses, we propose a model for the role of LPD-3 in *C. elegans* (Fig. 4f). In this model, LPD-3

spans the ER and PM at localized membrane contact sites and acts as a megaprotein-based molecular bridge that mediates non-vesicular ER-to-PM trafficking of phospholipids. Such non-vesicular and rapid mode of lipid trafficking may be particularly important for meeting the demand of membrane expansion during development and for membrane fluidity adjustment during physiological adaptation to cold stress in adulthood. LPD-3-mediated proper flow of phospholipids from the ER to PM also ensures appropriate levels of PC in ER membranes that, in turn, control the ER-to-nuclear translocation of SBP-1. In the nucleus, SBP-1 can regulate the expression of genes including *fat-7* and others involved in lipogenesis, metabolic homeostasis, membrane property regulation and stress responses[21,24,25,35] (Fig. 4f).

We found striking rescue of all examined phenotypic defects of *lpd-3* mutants by exogenous supplementation of phospholipids or Lecithin. Ineffective rescue by phospholipid head group constituents or fatty acids indicates that phospholipid/Lecithin may act by incorporating into host membranes rather than providing simple nutritional support. Unlike eukaryote-derived polyunsaturated phospholipids, bacterial phospholipids from *E. Coli*, which *C. elegans* feeds on, contain little PC and mostly saturated lipids[51] thus failing to support proper development and adult adaptation to cold in *lpd-3* mutants. Although our results suggest critical roles of LPD-3 in ER-to-PM lipid trafficking, LPD-3 may also localize and function at membrane contact sites formed by other ER-associated organelles[14]. Along with the recently described family of VPS13/ATG2 lipid transporters, LPD-3 may represent an emerging class of lipid transporters that serve as molecular “highway bridges” critical for directed non-vesicular trafficking of lipids across different organelle membranes[12–16]. Although our data strongly support diverse phospholipids with unsaturated acyl chains as transported substrates by LPD-3, the precise substrate specificity and biophysical mechanisms of transport await further investigations.

Molecular functions of LPD-3 and its evolutionarily conserved orthologues have remained hitherto unknown. Its yeast orthologue Csf1 has been implicated in cold tolerance[52]. The *Drosophila* homologue Tweek regulates synaptic functions and PIP2 levels[53]. Mutations in the human orthologue KIAA1109 cause Alkuraya-Kucinskas syndrome, a neuro- and cardiovascular development disorder with no known medical treatment[17–19,54]. Loss of KIAA1109 also impairs phagocytosis of *L. pneumophila* by macrophages[55]. These divergent phenotypes may be underpinned by a unifying conserved role of this protein family in lipid trafficking. Rescue of *lpd-3* mutants in *C. elegans* by Lecithin suggests a similar route to treat the Alkuraya-Kucinskas syndrome. Potentially conserved roles of KIAA1109 and other mammalian homologues of LPD-3 in regulating lipid trafficking and lipogenesis also raise the possibility of targeting KIAA1109 in diverse lipid metabolic disorders, including fatty liver diseases and obesity.

Methods

C. elegans

C. elegans strains were maintained with laboratory standard procedures unless otherwise specified. The N2 Bristol strain was used as the reference wild type, and the polymorphic Hawaiian strain CB4856 was used for genetic linkage mapping and SNP analysis[56,57]. Forward genetic screens for *fat-7*p::GFP activating or suppressing mutants after ethyl methanesulfonate (EMS)-induced random mutagenesis were performed as described previously[3,58]. Approximately 25,000 haploid genomes were screened for *acdh-11* suppressors, yielding at least 18 independent mutants. Identification of mutations by whole-genome sequencing and complementation tests by crossing EMS mutants with *lpd-3(ok2138)* heterozygous males were used to determine *dma533*

and *dma544* as alleles of *lpd-3*. Feeding RNAi was performed as previously described[59]. Transgenic strains were generated by germline transformation as described[60]. Transgenic constructs were co-injected (at 10 - 50 ng/μl) with dominant *unc-54p*::mCherry or GFP, and stable extrachromosomal lines of fluorescent animals were established. Genotypes of strains used are as follows: Chr. I: *lpd-3(dma533, 544, ok2138)*, Chr. III: *acdh-11(n5857);* Chr. IV: *cka-1(dma550)*, Chr. V: *nIs590[fat-7::GFP]*, Chr. X: *sams-1(dma553, ok3033), dmaEx647 [rpl-28p::lpd-3 Nt::mCherry; unc-54p::GFP], dmaEx648 [ges-1p:: mCherry::lpd-3 Ct; unc-54p::GFP], epEx141 [sbp-1p::GFP::sbp-1 + rol-6(su1006)], pwIs503 [vha-6p::mans::GFP + Cbr-unc-119(+)], hjIs73 [vha-6p::GFP::daf-22 + C. briggsae unc-119(+)], xmSi01[mai-2p::mai-2::GFP]; epIs14 [sbp-1p::GFP + rol-6(su1006)], pwIs890[Pvha-6::AKT(PH)::GFP], jyIs13 [act-5p::GFP::act-5 + rol-6(su1006)], zcIs4 [hsp-4::GFP]*.

Structural prediction of LPD-3

The full-length LPD-3 was split into eight fragments, each with ~ 1,000 residues. Each fragment has ~ 500 overlapping residues with the neighboring fragments. Structure prediction of each fragment was generated by Uni-fold (https://hermite.dp.tech/), a modified AlphaFold v2.0 program[37]. Predicted structures were aligned using Chimera[61] based on the overlapping sequence. Then, the aligned structures of all fragments were merged in Coot[62] to obtain the full-length structure. Several flexible regions were manually adjusted. The structural images were prepared in ChimeraX[63].

Zebrafish

To investigate functions of *kiaa1109* in affecting cold resistance zebrafish larvae, the morpholino (MO) used to target zebrafish *kiaa1109* (E4I4) was obtained from Gene Tools[18]. Fertilized eggs of AB strain zebrafish were obtained as previously described[50]. The *kiaa1109* and ctrl MOs were

dissolved in ultrapure water (5 ng/nL) and 1-2 nL MO solution was injected into each zebrafish egg at single cell stage using a PICO-LITER injector from WARNER. The injected embryos were incubated in E3 medium at 28 ºC. The injected larvae with normal phenotype were selected and exposed to 10 ºC at 96 hpf. After 24 hours of cold exposure, the larvae were let to recover at 28 ºC for 24 h. The fish were checked frequently and the dead ones were removed and counted. At the end of the experiment, the survived fish were classified as abnormal and normal as previously reported[50]. Photographs of the larvae before and after cold exposure were taken using a Zeiss stereomicroscope equipped with a color CCD camera. Body length of the larvae was measured by analyzing the photographs using AxioVision (v-4.8).

Sample preparation for RNA sequencing, qRT-PCR and data analysis

N2 and *lpd-3*(*ok2138)* animals were maintained at 20 °C and washed down from NGM plates using M9 solution and subjected to RNA extraction using TissueDisruptor and the RNeasy Mini Kit from Qiagen. RNA preparations were used for qRT-PCR or RNAseq. For qRT-PCR, reverse transcription was performed by SuperScript III, and quantitative PCR was performed using LightCycler Real-Time PCR Instruments. Relative mRNA levels were calculated by ΔΔCT method and normalized to actin. Primers for qRT-PCR: *act-3* (forward, tccatcatgaagtgcgacat; reverse, tagatcctccgatccagacg) and *fat-7* (forward, tgcgttttacgtagctggaa; reverse, caccaacggctacaactgtg). RNAseq library preparation and data analysis were performed as previously described[28]. Three biological replicates were included for each treatment. The cleaned RNAseq reads were mapped to the genome sequence of *C. elegans* using hisat2[64]. Abundance of genes was expressed as FPKM (Reads per kilobase per million mapped reads). Identification of differentially expressed genes was performed using the DESeq2 package[65].

***C. elegans* cold and freezing stress and rescue by phospholipid/Lecithin**

Animals were cultured under non-starved conditions for at least 4 generations before cold and freezing resilience assays. For cold resilience assay, bleach-synchronized L4 populations were kept at 4 °C for 20 hrs and then recovered for 24 hrs at 25 °C. For freezing resilience assay, bleach-synchronized L4 populations were kept at -20 °C for 45 mins and then recovered for 24 hrs at 25 °C. For both cold and freezing experiments, NGM plates spread with equal agar thickness seeded with equal amounts of OP50 were used while cold and freezing temperature readings were monitored by thermometers to ensure minimal fluctuation. After cold or freezing shock, animals were moved to 25 °C for recovery and scored as dead if they showed no pumping and movement upon light touch with the body necrosis subsequently confirmed by light microscopy. For phospholipid and Lecithin rescue experiments, phospholipid (11145, Sigma-Aldrich), Lecithin (O3376-250, Fisher Chemical) or PC (P5394-10G, Sigma-Aldrich) was prepared as mixture by dissolving in M9 solution (from 1 to 20 mg/ml) and thorough vortexing. Phospholipids or Lecithin mixtures were then added (200 µl/ 60 cm plate) on NGM plates with pre-seeded OP50 and dried briefly before placing animals for cold or freezing tolerance assays.

C. elegans development, fecundity and behavioral assays

To assay the developmental delay of *lpd-3* mutants, developmentally synchronized embryos from bleaching of gravid adult wild-type and *lpd-3* mutant hermaphrodites were plated on NGM plates and grown at 20 ^{o}C. After indicated duration (40, 45 and 50 hrs), percentages of animals reaching the L4 stage (with characteristic crescent vulvar structures) were quantified. To assay fecundity, single L4 worm was placed to control, phospholipid (20 mg/ml) and Lecithin (20mg/ml) containing plates (prepared as above). After 72 hrs, the total number of progenies at all stages was scored. For locomotion behavioral assays, the average speed of worms was recorded for synchronized young adult hermaphrodite (24 hrs post L4) using WormLab System

(MBF Bioscience) based on the midpoint position of the worms[66]. Each experiment was repeated at least 3 times as independent biological replicates with more than 10 animals per group.

Confocal and epifluorescence microscopic imaging

SPE confocal and epifluorescence compound microscopes (Leica) were used to capture fluorescence images. Animals of different genotypes were randomly picked at the same young adult stage (24 hrs post L4) and treated with 1 mM Levamisole sodium Azide in M9 solution (31,742-250MG, Sigma-Aldrich), aligned on an 4% agar pad on slides for imaging. Identical setting and conditions were used to compare genotypes, experimental groups with control.

Mammalian cell culture experiments

MEFs were derived from *Kiaa1109* mutant mice [B6N(Cg)-4932438A13Rik$^{tm1b(EUCOMM)Hmgu}$/J, Stock No.026878] generated by the Knockout Mouse Project (KOMP) at The Jackson Laboratory (Bar Harbor, Maine, USA) using embryonic stem cells provided by the International Knockout Mouse Consortium. *Kiaa1109*$^{-/-}$ embryos were obtained from interbreeding of heterozygotes. *Kiaa1109* mice were genotyped using the following PCR primers: wild-type allele (380bp) forward GGG ATA TGG CAG AGA AGC TG, reverse AAA ACA ATT GGC TTA GAG ACT TCA; mutant allele forward CGG TCG CTA CCA TTA CCA GT, reverse GAC CAC ACA AAT CCC TTG GT. MEFs were cultured in DMEM (Thermo Fisher Scientific, MT-10–013-CV), supplemented with 10% FBS (Gemini Bio-Products, 900–208) and 1% penicillin/streptomycin and early passages (P2 - P5) were used for reporter transfection, PC lipid labeling and cold resilience experiments. For phospholipid reporter transfection, MEFs were seeded at density of 4 x 105 cells/ml in 12-well plates containing glass cover slips and grown to 70-90% confluency. Mixture of DMEM, PloyJet reagent (Signagen Laboratories, MD, US) and

CMVp::AKT-PH::GFP plasmids (Addgene) were prepared and added to wild-type and *Kiaa1109* KO MEF cultures, followed by imaging with fluorescence confocal microscopy after 48 hrs.

U937 cells (as suspension cultures) from ATCC were cultured in RPMI-40 (Gibco) medium supplemented with 10% heat-inactivated FBS (Hyclone), penicillin (10,000 I.U./mL), streptomycin (10,000 g/mL). HEK293T cells (as adherent cultures) were cultured in DMEM (Thermo Fisher Scientific, MT-10–013-CV), supplemented with 10% FBS (Gemini Bio-Products, 900–208) and 1% penicillin/streptomycin. Both cell lines were maintained in a humidified 5% CO2 incubator at 37 °C. U937 cells expressing lentiCas9-Blast were used to generate clonal lines of KIAA1109 KO with the sgRNAs targeting sequences GCCAGCTACCCCCGAATAtgg and GTTGACATCTACTACTACAtgg. For cold stress experiments, parental control and KIAA1109 KO U937 cells were cold shocked (4 ^{o}C for 20 hrs) and assayed for cell death using CYTOX Green-based flow cytometry. For lipid reporter experiments, HEK293 cells were co-transfected with plasmids with AKT-PH::GFP and shRNA against *KIAA1109* (Sigma-Aldrich, TRCN0000263343 with 73% knockdown efficiency), incubated for 48 hrs and imaged by confocal microscopy for membrane localized GFP.

Lipid metabolic labeling with propargylcholine

For PC lipid labelling in MEFs, *Kiaa1109*$^{+/+}$ and *Kiaa1109*$^{-/-}$ MEFs were incubated with propargylcholine (100 μM) in complete media for 24 hrs, fixed with 4% PFA in PBS for 5 mins, reacted with 100 μM Alexa-488 Azide for 30 mins. The cells were washed with PBS and imaged with fluorescence confocal microscopy. For PC lipid labelling in *C. elegans*, wild type and *lpd-3* mutants were cultured under non-starved conditions for at least 4 generations. L4-stage animals were incubated with 100 μM propargylcholine in OP50 culture for 24 hrs at 20 ^{o}C, fixed with 4%

PFA in PBS for 5 mins, reacted with 100 μM Alexa-488 Azide for 30 mins, washed with PBS and imaged with fluorescence confocal microscopy.

Statistical analysis

Data were analyzed using GraphPad Prism 9.2.0 Software (Graphpad, San Diego, CA) and presented as means ± S.D. unless otherwise specified, with *P* values calculated by unpaired two-tailed t-tests (comparisons between two groups), one-way or two-way ANOVA (comparisons across more than two groups) and adjusted with Bonferroni's corrections.

Data availability

The RNAseq read datasets were deposited in NCBI SRA (Sequence Read Archive) under the BioProject accession PRJNA827259. All other data generated for this study are included in this article.

Acknowledgments

Some strains were provided by Drs. Barth Grant, Rosa E. Navarro González, and *Caenorhabditis* Genetics Center (CGC), which is funded by NIH Office of Research Infrastructure Programs (P40 OD010440). The work was supported by NIH grant 1R35GM139618, UCSF PBBR New Frontier Research (NFR) and the Packard Fellowship in Science and Engineering (D.K.M).

Author contributions

C.W., B.W. and D.K.M. designed, performed and analyzed most of the *C. elegans* experiments and wrote the manuscript. Y.L. performed RNAseq bioinformatic analysis and Zebrafish experiments. T.P., F.O., R.G. and J.S. performed genetic mapping experiments and whole-genome sequencing analysis. J.Z. performed structural analysis. C.V. and J.M. contributed to

446 lipid analysis. H.D. and K.S. contributed to imaging analysis. M.B., S.M., Y.L. contributed to the

447 KIAA1109 sgRNA and KO cell experiments. D.K.M. supervised the project.

448 **Competing interests**

449 The authors declare no competing interests.

450 **Materials & Correspondence.**

451 Correspondence and material requests should be addressed to Dengke K. Ma, Ph.D.

452 (dengke.ma@ucsf.edu).

453 **Figures and Figure legends**

Figure 1

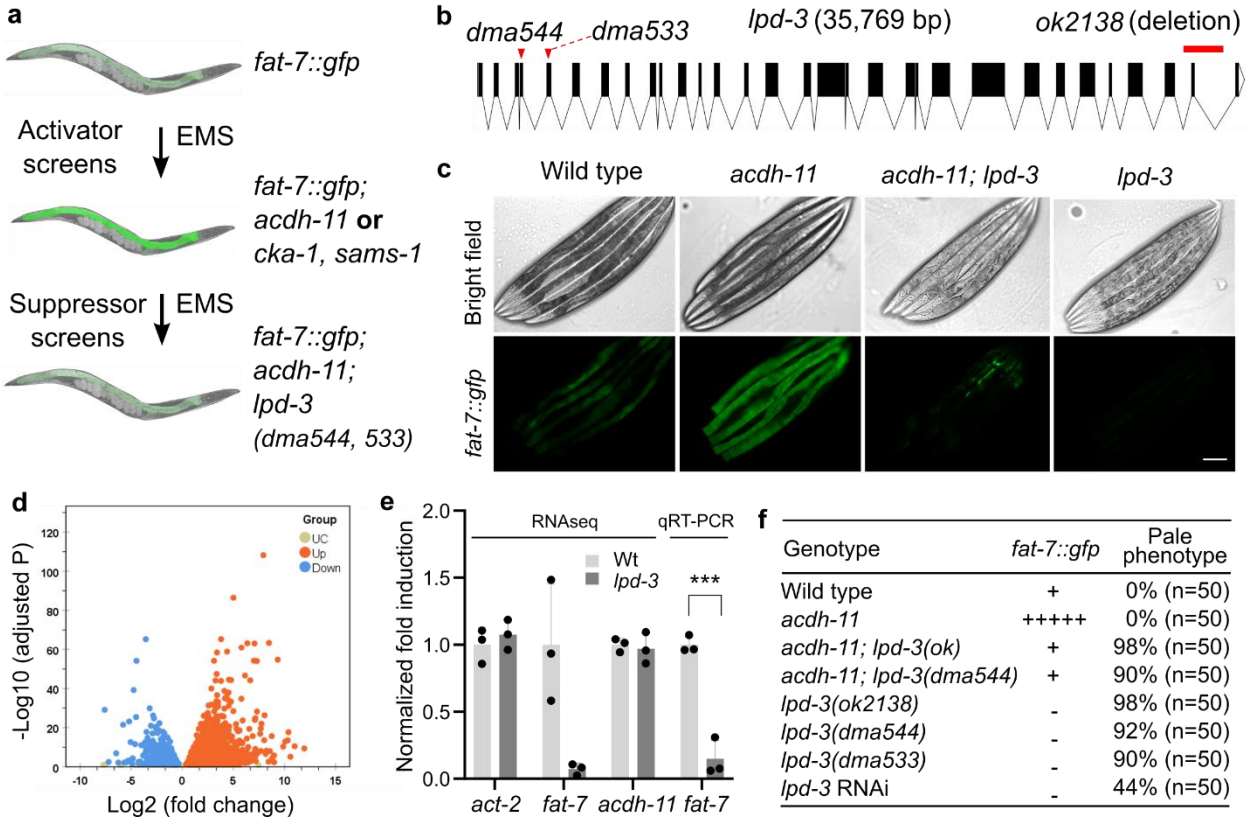

Genotype	*fat-7::gfp*	Pale phenotype
Wild type	+	0% (n=50)
acdh-11	+++++	0% (n=50)
acdh-11; lpd-3(ok)	+	98% (n=50)
acdh-11; lpd-3(dma544)	+	90% (n=50)
lpd-3(ok2138)	-	98% (n=50)
lpd-3(dma544)	-	92% (n=50)
lpd-3(dma533)	-	90% (n=50)
lpd-3 RNAi	-	44% (n=50)

454

Fig. 1. Genetic identification and transcriptomic analysis of *lpd-3*. a, Schematic of genetic screens that led to the identification of *acdh-11*, *cka-1*, and *sams-1* as negative regulators of *fat-7* and *acdh-11*-suppressing *lpd-3* as positive regulator of *fat-7*. **b**, Full-length gene diagram of *lpd-3* with the point mutations *dma544*, *dma533* (arrows) and deletion mutation *ok2138* (line). **c**, Representative images of *fat-7*::GFP animals in wild type, *acdh-11(n5857)* single, *acdh-11(n5857); lpd-3(ok2138)* double, or *lpd-3(ok2138)* single mutants. Scale bar, 50 μm. **d**, Volcano plot showing significantly (adjusted p value < 0.05) up- (green) or down- (blue) regulated genes in *lpd-3* mutants compared with wild type. **e**, Normalized fold induction (RNAseq and qRT-PCR) of *fat-7* showing its diminished expression in *lpd-3* mutants. Values are means ± S.D. ***P < 0.001 (N = 3 biological replicates). **f**, Table summary of *fat-7*::GFP abundance (indicated by relative numbers of plus signs based on fluorescent intensities or minus sign, no signals) and the morphological pale phenotypes in animals with indicated genotypes (single, double mutations or RNAi) and phenotypic penetrance.

Figure 2

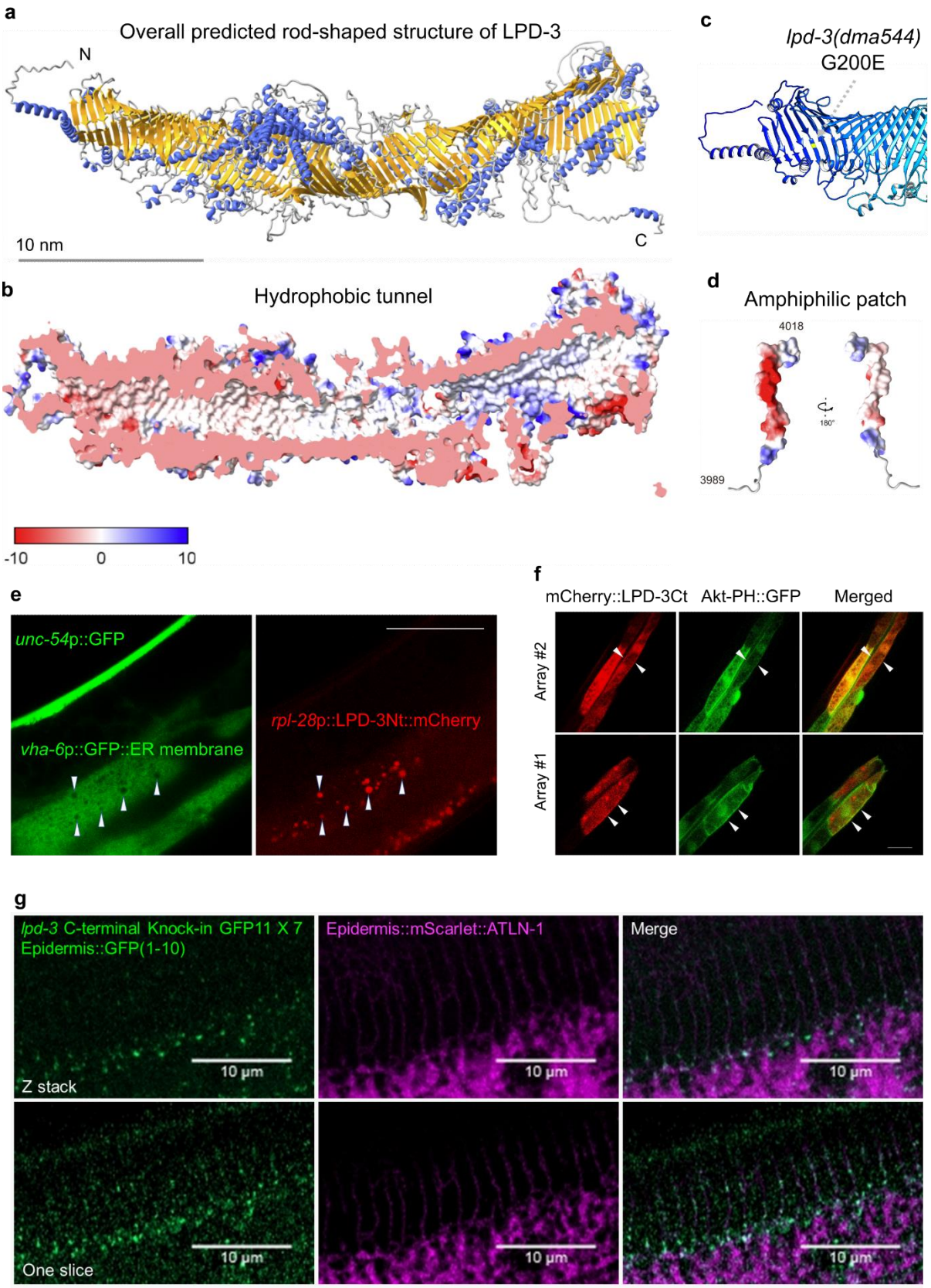

Fig. 2. Structural features and cellular localizations of LPD-3. a, Overall structure of the full-length LPD-3 assembled from eight segments whose structures were separately predicted by AlphaFold v2.0, with both N and C-termini noted. **b**, Cross-sectional view of the LPD-3 structure showing the hydrophobic tunnel running continuously along the entire inside. **c**, Ribbon representation of the N-terminal part of LPD-3, with the G200E mutation indicated in yellow. **d**, Structure of the LPD-3 C-terminus showing an amphiphilic patch (hydrophobic, red; hydrophilic, blue) that was used to generate mCherry-fused LPD-3 reporters. **e**, Representative fluorescence images showing co-localization (arrow heads) of ER membrane markers with a mCherry fusion reporter of the LPD-3 N-terminus (*rpl-28*p:: LPD-3Nt::mCherry with LPD-3 a.a. 1-72, *unc-54*p::GFP as co-injection marker). **f**, Representative fluorescence images (from two independent transgenic extrachromosomal arrays #1 and #2) showing co-localization (arrow heads) of AKT-PH::GFP that binds to PM-PIP2/PIP3 with a mCherry fusion reporter (*ges-1*p::mCherry::LPD-3Ct, a.a. 3945-4018) of the LPD-3 C-terminus. Scale bar, 50 µm. **g**, Representative confocal fluorescence images showing endogenous LPD-3::GFP (generated by CRISPR/Cas9-mediated knock-in) in apposition with mScarlet::ATLN-1, a tubular ER marker.

Figure 3

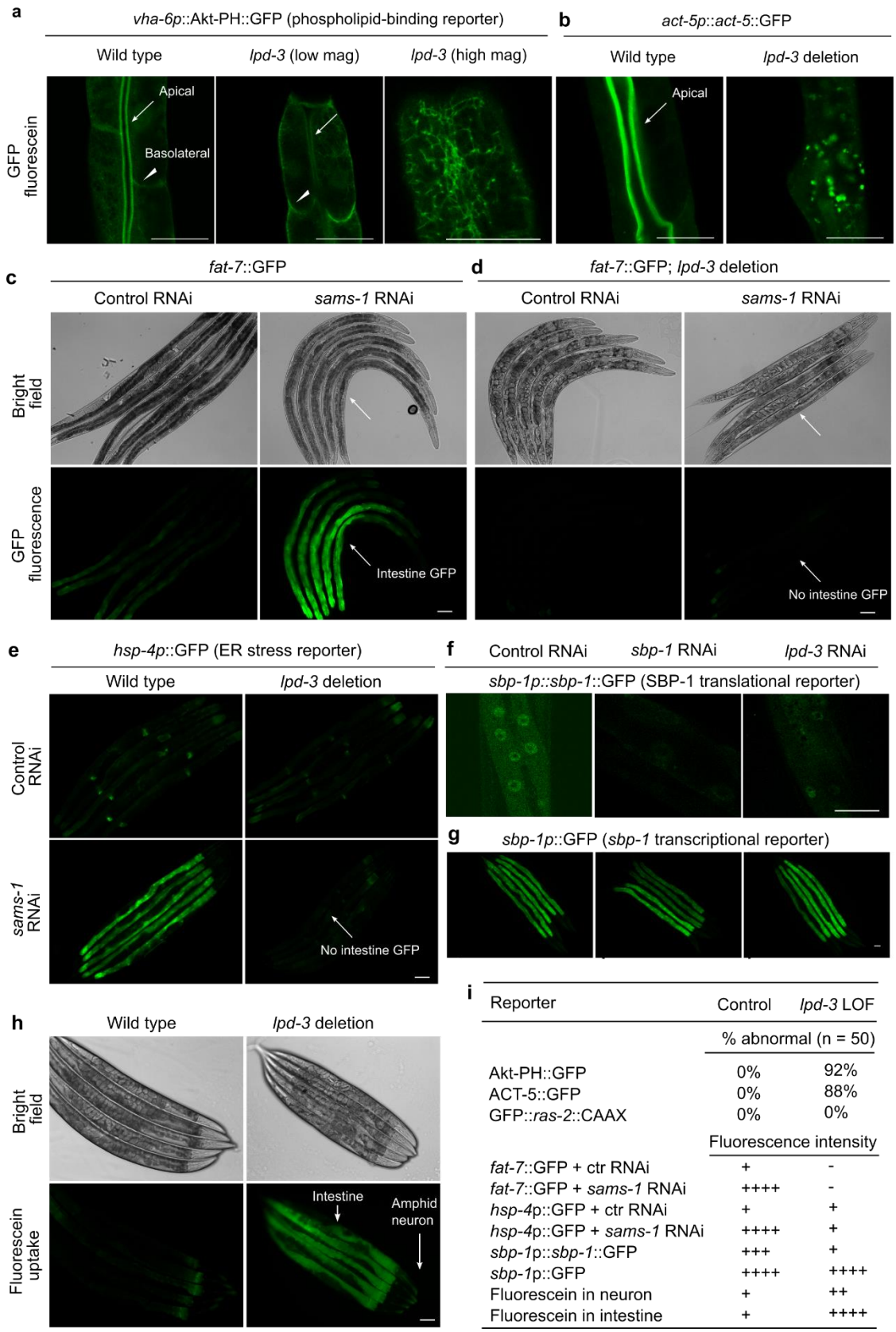

i

Reporter	Control	*lpd-3* LOF
	% abnormal (n = 50)	
Akt-PH::GFP	0%	92%
ACT-5::GFP	0%	88%
GFP::*ras-2*::CAAX	0%	0%
	Fluorescence intensity	
fat-7::GFP + ctr RNAi	+	-
fat-7::GFP + *sams-1* RNAi	++++	-
*hsp-4*p::GFP + ctr RNAi	+	+
*hsp-4*p::GFP + *sams-1* RNAi	++++	+
*sbp-1*p::*sbp-1*::GFP	+++	+
*sbp-1*p::GFP	++++	++++
Fluorescein in neuron	+	++
Fluorescein in intestine	+	++++

Fig. 3. Essential roles of LPD-3 in ER-to-PM lipid trafficking and SBP-1 regulation. a, Representative confocal fluorescence images showing PIP2/PIP3-binding Akt-PH::GFP reporters in wild type (apical intestinal membrane, arrow; basolateral membrane, arrow head) and *lpd-3(ok2138)* mutants at both low and high magnifications. **b**, Representative confocal fluorescence images showing the actin reporter *act-5p::act-5::GFP* in wild type (apical intestinal membrane, arrow) and *lpd-3(ok2138)* mutants. **c**, Representative bright-field and epifluorescence images showing activation of *fat-7*::GFP by RNAi against *sams-1*. **d**, Representative bright-field and epifluorescence images showing activation of *fat-7*::GFP by RNAi against *sams-1* in wild type but not *lpd-3(ok2138)* mutants (arrow). **e**, Representative epifluorescence images showing activation of the *hsp-4*p::GFP ER stress reporter by RNAi against *sams-1* in wild type but not *lpd-3(ok2138)* mutants (arrow). **f**, Representative confocal fluorescence images showing reduced abundance of nuclear *sbp-1*p::*sbp-1*::GFP by RNAi against *sbp-1* or *lpd-3*. **g**, Representative epifluorescence images showing no apparent changes of *sbp-1*p::GFP by RNAi against *sbp-1* or *lpd-3*. **h**, Representative epifluorescence images showing markedly increased membrane permeability for fluorescein in *lpd-3*(*ok2138*) mutants. **i**, Table summary of reporter phenotypes of indicated genotypes or conditions. Scale bars, 50 μm.

Figure 4

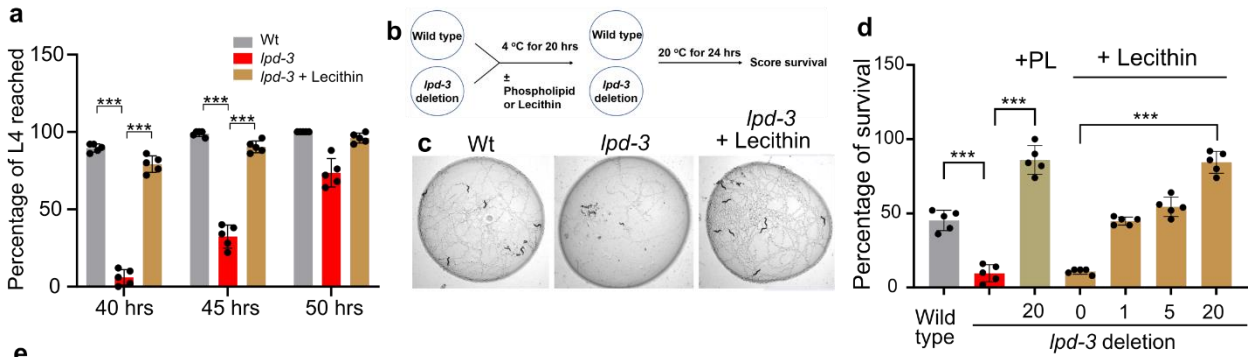

e

Phenotype	Wild type	*lpd-3*	*lpd-3* + Lecithin
Development	+++++	++	+++++
Fecundity	+++++	+	+++
Locomotion	+++++	+++	++++
Lipid droplet	+++++	++	++++
Membrane integrity	+++++	+	+++++
Cold stress resilience	+++++	+	++++

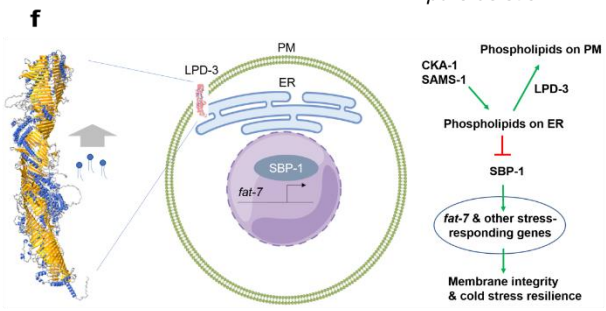

Fig. 4. Phospholipid/Lecithin rescues phenotypes of *C. elegans lpd-3* mutants. a, Percentages of animals that reached developmental L4 stage at indicated hours post egg preparation in wild type, *lpd-3(ok2138)* mutants with or without supplementation of Lecithin since egg preparation. **b**, Schematic of the experiment to measure cold resilience of wild type and *lpd-3(ok2138)* mutants with supplementation of soy phospholipids or Lecithin for 6 hrs post developmental L4 stage. **c**, Representative bright-field images showing markedly decreased survival of *lpd-3(ok2138)* mutants against cold exposure (4 ºC for 20 hrs) and rescued survival by Lecithin supplementation. **d**, Percentages of survived animals against cold exposure (4 ºC for 20 hrs) with indicated genotypes and increasing doses of Lecithin or soy phospholipids (PL) that rescued *lpd-3* mutants. **e**, Table summary of observed *lpd-3* phenotypes and their degrees of rescue (indicated by the numbers of + signs) by Lecithin (1 mg/ml on NGM). **f**, Model to illustrate molecular functions of LPD-3 in mediating non-vesicular ER-to-PM lipid trafficking, antagonizing effects of CKA-1 and SAMS-1 on lipids at ER membranes, and regulation of genes including *fat-7*

515 through SBP-1. Other components of the pathway are omitted for clarity. Values are means ±
516 S.D with ***P < 0.001 (N = 5 independent experiments, n > 50 animals per experiment).

Figure 5

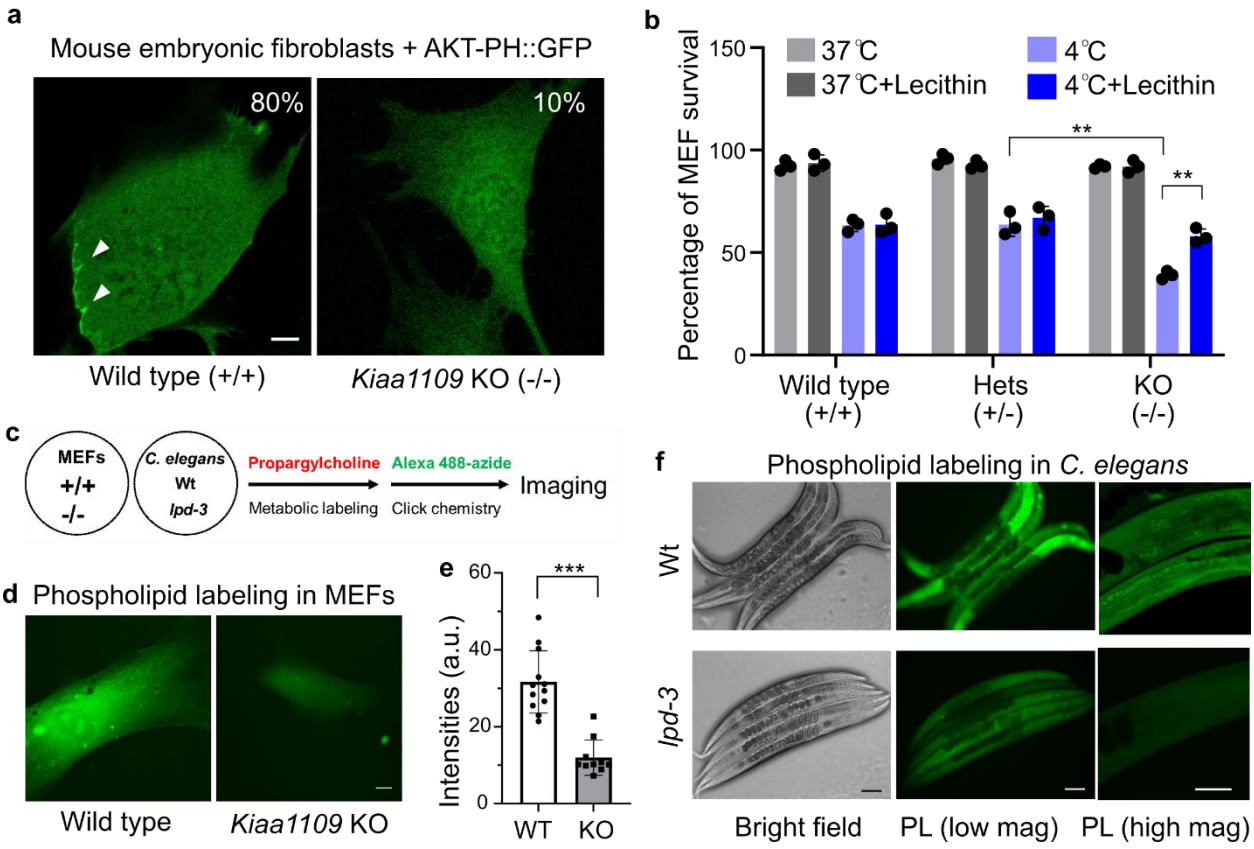

517

518 **Fig. 5. Conserved roles of the LPD-3 homologue Kiaa1109 in MEFs. a**, Representative
519 confocal fluorescence images showing enriched AKT-PH::GFP localization to ruffling
520 membranes at cell periphery in wild-type (80%, n = 20) but not *Kiaa1109* KO (0%, n = 20)
521 MEFs. **b**, Quantification of cell survival rates of MEFs based on SYTOX blue staining with
522 indicated genotypes (wild type, heterozygous and homozygous knock-out of *Kiaa1109* in MEFs)
523 after cold stress treatment. Values are means ± S.D with **P < 0.01 (N = 3 independent
524 experiments, n > 700 cells per experiment). **c**, Schematic of metabolic phospholipid labeling
525 using propargylcholine and click chemistry for visualization. **d**, Representative confocal

526 fluorescence images showing typical enriched propargylcholine staining signals with Alexa-488
527 fluorescence in wild-type and *Kiaa1109* KO MEFs. **e**, Quantification of Alexa-488 fluorescence
528 intensities (a.u., arbitrary unit) of propargylcholine-labelled phospholipids in wild-type and
529 *Kiaa1109* KO MEFs. Values are means ± S.D with ***$P < 0.001$ ($n > 10$ cells from independent
530 experiments). **f**, Representative bright field and fluorescence images showing typical enriched
531 propargylcholine staining signals in wild type and *lpd-3(ok2138)* mutants. Scale bars, 50 µm.

Extended Data Figure 1

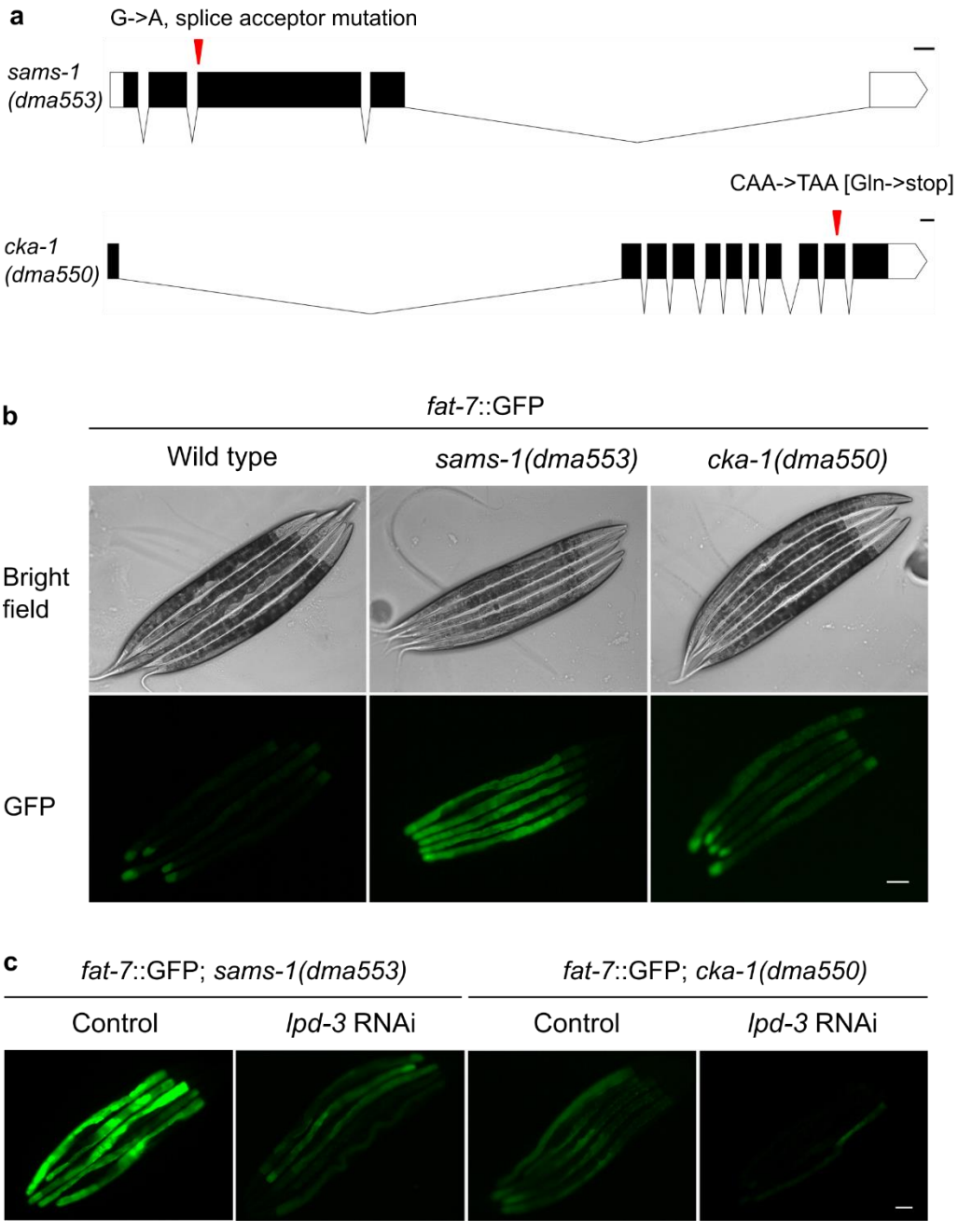

Extended Data Fig. 1. Genetic identification of *cka-1* and *sams-1* in regulating *fat-7*::GFP.

a, Gene diagrams showing *sams-1*(*dma553*) and *cka-1*(*dma550*) that cause a splice acceptor mutation and a premature stop codon mutation, respectively, identified by WGS. **b**, Representative bright-field and epifluorescence images showing activation of *fat-7*::GFP by

537 *sams-1*(*dma553*) and *cka-1*(*dma550*). Both mutations were isolated from EMS screens and
538 outcrossed at least 5 times, segregating with *fat-7*::GFP activation phenotypes. **c**, Representative
539 epifluorescence images showing that RNAi against *lpd-3* attenuated activation of *fat-7*::GFP by
540 *sams-1*(*dma553*) or *cka-1*(*dma550*). Scale bar: 50 µm.

Extended Data Figure 2

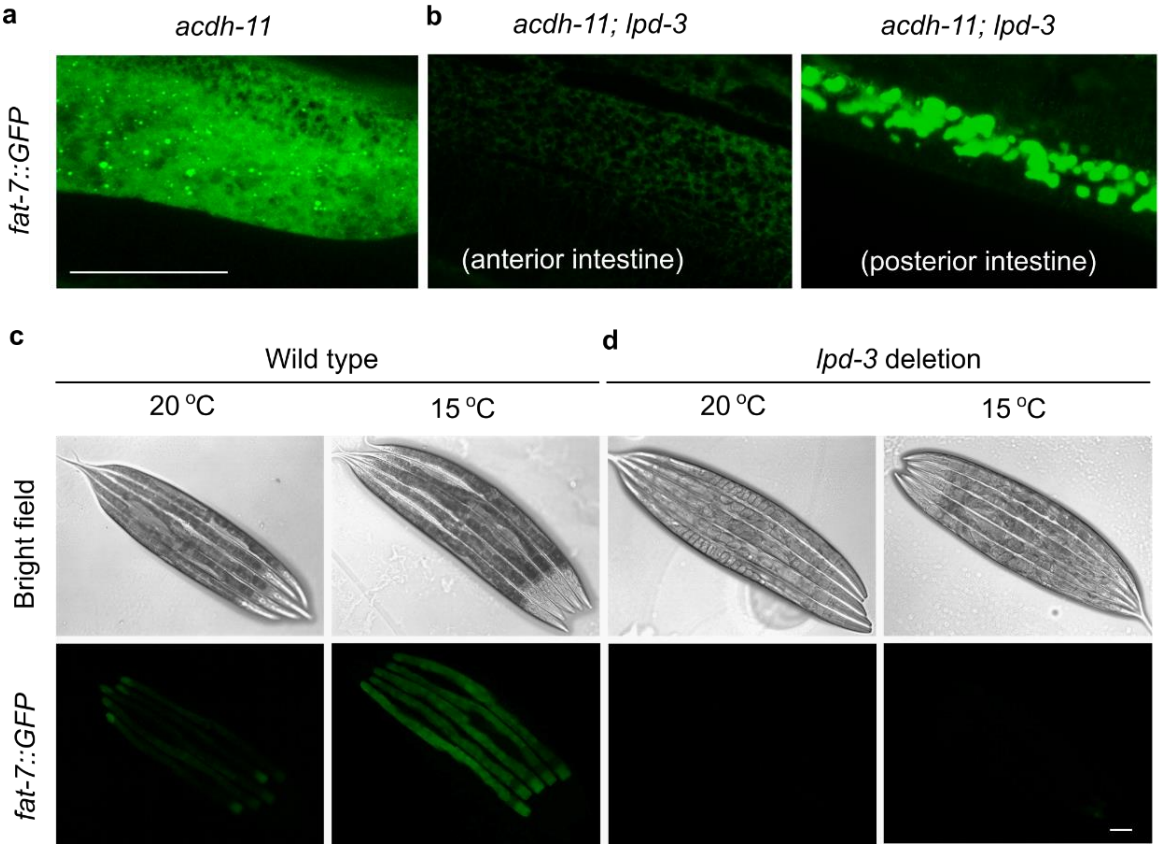

541

542 **Extended Data Fig. 2. *lpd-3* suppresses *acdh-11* or hypothermia-induced *fat-7*::GFP. a**,
543 Confocal fluorescence image (Z-stack) showing *fat-7*::GFP in *acdh-11(n5857)* mutants. **b**,
544 Confocal fluorescence images showing *lpd-3(ok2138)* deletion mutation suppresses *fat-7*::GFP
545 in *acdh-11(n5857)* mutants, more prominently in the anterior than posterior intestine. **c**, Bright
546 field and epifluorescence images showing up-regulation of *fat-7*::GFP by hypothermia (15 °C 24

547 hrs). **d**, Bright field and epifluorescence images showing up-regulation of *fat-7*::GFP by

548 hypothermia (15 ºC 24 hrs) is blocked in *lpd-3(ok2138)* deletion mutants. Scale bar: 50 µm.

549

Extended Data Figure 3

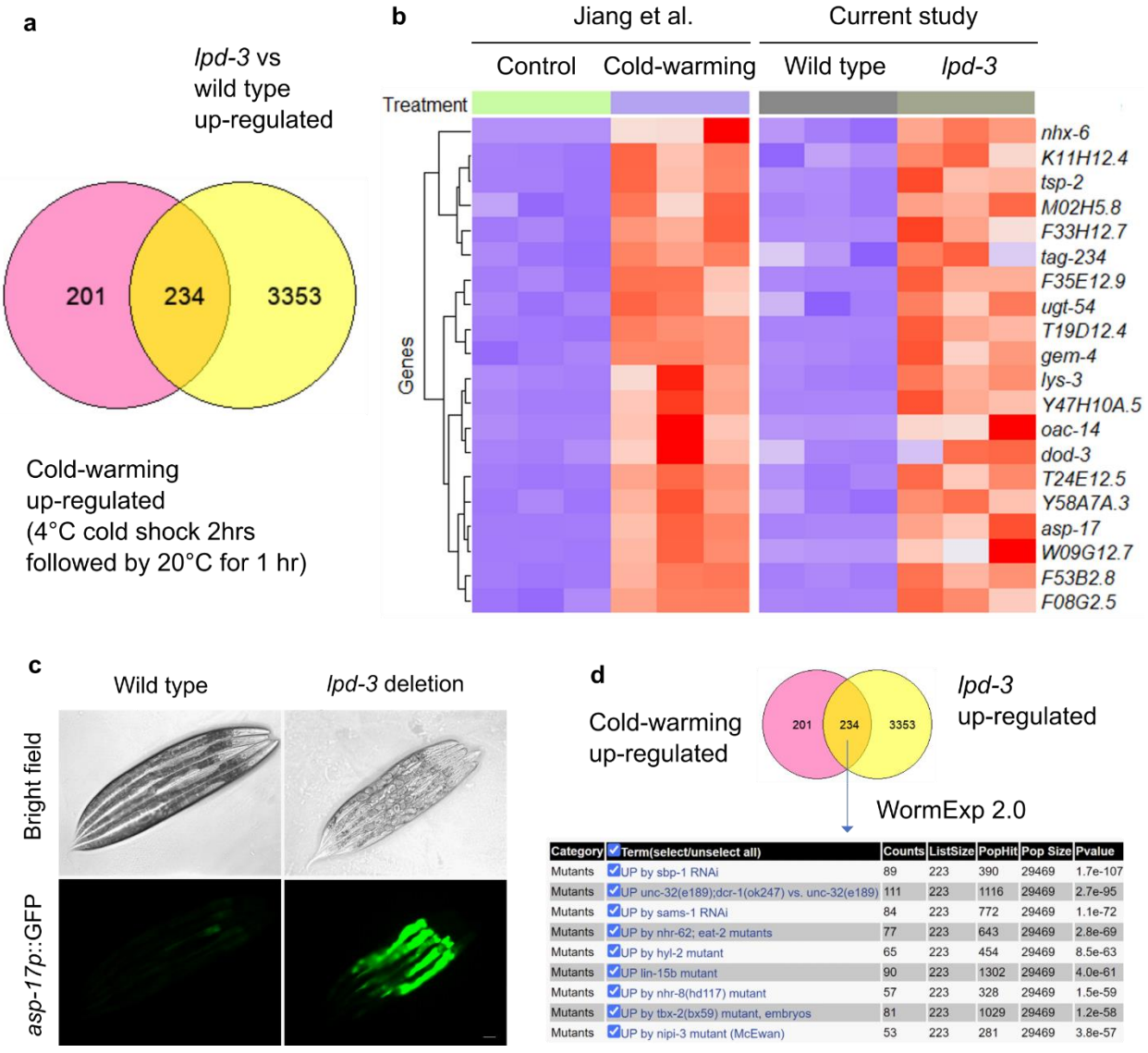

Category	Term(select/unselect all)	Counts	ListSize	PopHit	Pop Size	Pvalue
Mutants	UP by sbp-1 RNAi	89	223	390	29469	1.7e-107
Mutants	UP unc-32(e189);dcr-1(ok247) vs. unc-32(e189)	111	223	1116	29469	2.7e-95
Mutants	UP by sams-1 RNAi	84	223	772	29469	1.1e-72
Mutants	UP by nhr-62; eat-2 mutants	77	223	643	29469	2.8e-69
Mutants	UP by hyl-2 mutant	65	223	454	29469	8.5e-63
Mutants	UP lin-15b mutant	90	223	1302	29469	4.0e-61
Mutants	UP by nhr-8(hd117) mutant	57	223	328	29469	1.5e-59
Mutants	UP by tbx-2(bx59) mutant, embryos	81	223	1029	29469	1.2e-58
Mutants	UP by nipi-3 mutant (McEwan)	53	223	281	29469	3.8e-57

550

551 **Extended Data Fig. 3. RNAseq reveals genes commonly regulated by LPD-3, cold stress**

552 **and SBP-1. a**, Venn diagram showing commonly regulated genes by both *lpd-3(ok2138)* and

553 cold stress. **b**, Heat map showing the top 30 regulated genes by *lpd-3(ok2138)* that are also

554 regulated by cold stress. **c**, Bright field and epifluorescence images showing constitutive up-
555 regulation of *asp-17p::*GFP in *lpd-3(ok2138)* mutants. Scale bar: 50 µm. **d**, WormExp
556 (https://wormexp.zoologie.uni-kiel.de/wormexp/) analysis of *lpd-3* and cold-commonly regulated
557 genes showing they are most similar to the gene set regulated by RNAi against *sbp-1*.

558

Extended Data Figure 4

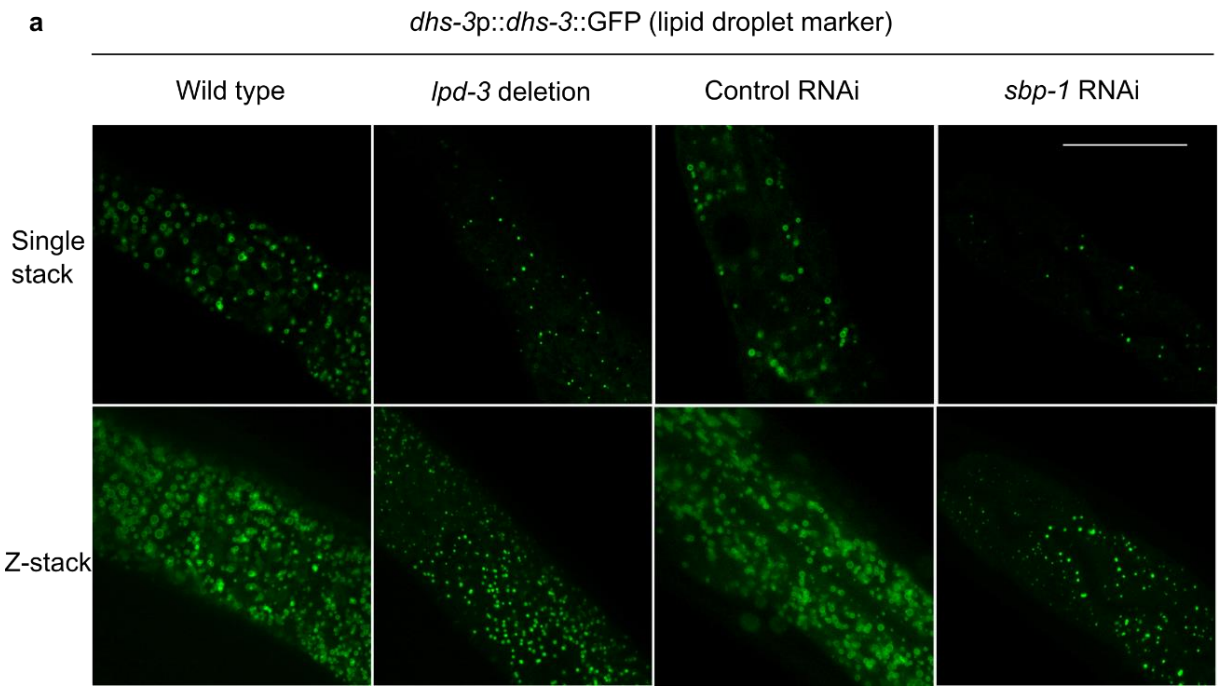

559

560 **Extended Data Fig. 4. *lpd-3* deletion causes lipid droplet defects as *sbp-1* RNAi does. a**,
561 Representative confocal fluorescence images (Single stack, above; Z-stack, below) showing that
562 both *lpd-3(ok2138)* and *sbp-1* RNAi can cause fewer in numbers and smaller in size of lipid
563 droplet makers *dhs-3*p::*dhs-3*::GFP. Scale bar: 50 µm.

Extended Data Figure 5

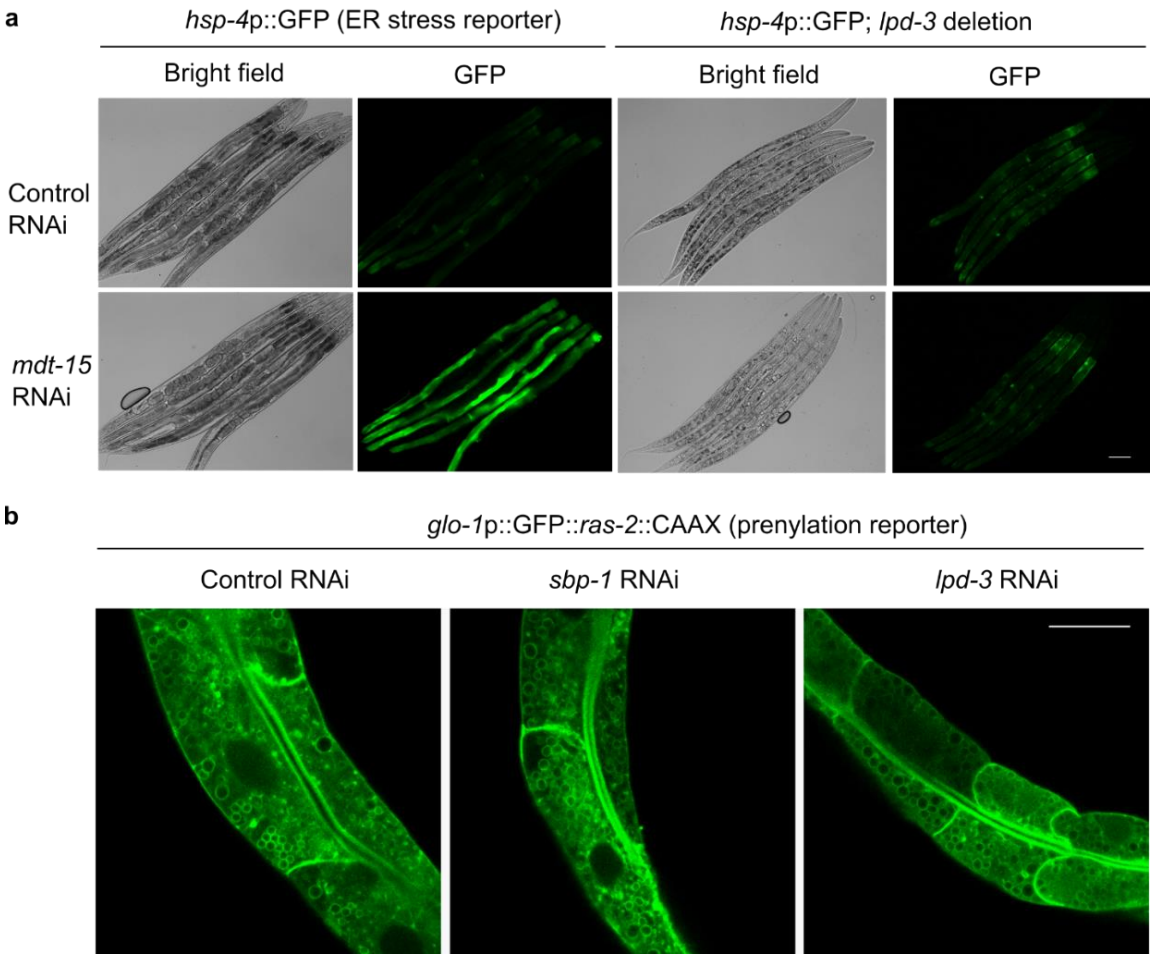

Extended Data Fig. 5. Additional evidence for specific roles of LPD-3 in the ER-to-PM trafficking of unsaturated lipids. a, Representative epifluorescence images showing activation of the *hsp-4*p::GFP ER stress reporter by RNAi against *mdt-15* in wild type but not *lpd-3(ok2138)* mutants. *mdt-15* RNAi activates *hsp-4*p::GFP because of reduced desaturase gene expression and excessive acyl chain saturation of ER membrane lipids[45]. **b,** Representative confocal fluorescence images showing largely normal intestinal PM morphology and PM-targeted trafficking of the prenylation reporter *glo-1*p::GFP::*ras-2*::CAAX in *sbp-1* or *lpd-3* RNAi-treated animals. Scale bar: 50 µm.

Extended Data Figure 6

a

Compounds	Rescue of *lpd-3* mutants
M9	-
M9 + Lecithin	++++
M9 + soy phospholipids	+++++
M9 + egg phospholipids	+++++
M9 + phosphotidylcholine	+++
M9 + choline	-
M9 + ethanolamine	-
M9 + serine	-
M9 + oleic acid salts	+
M9 + stearic acid salts	-

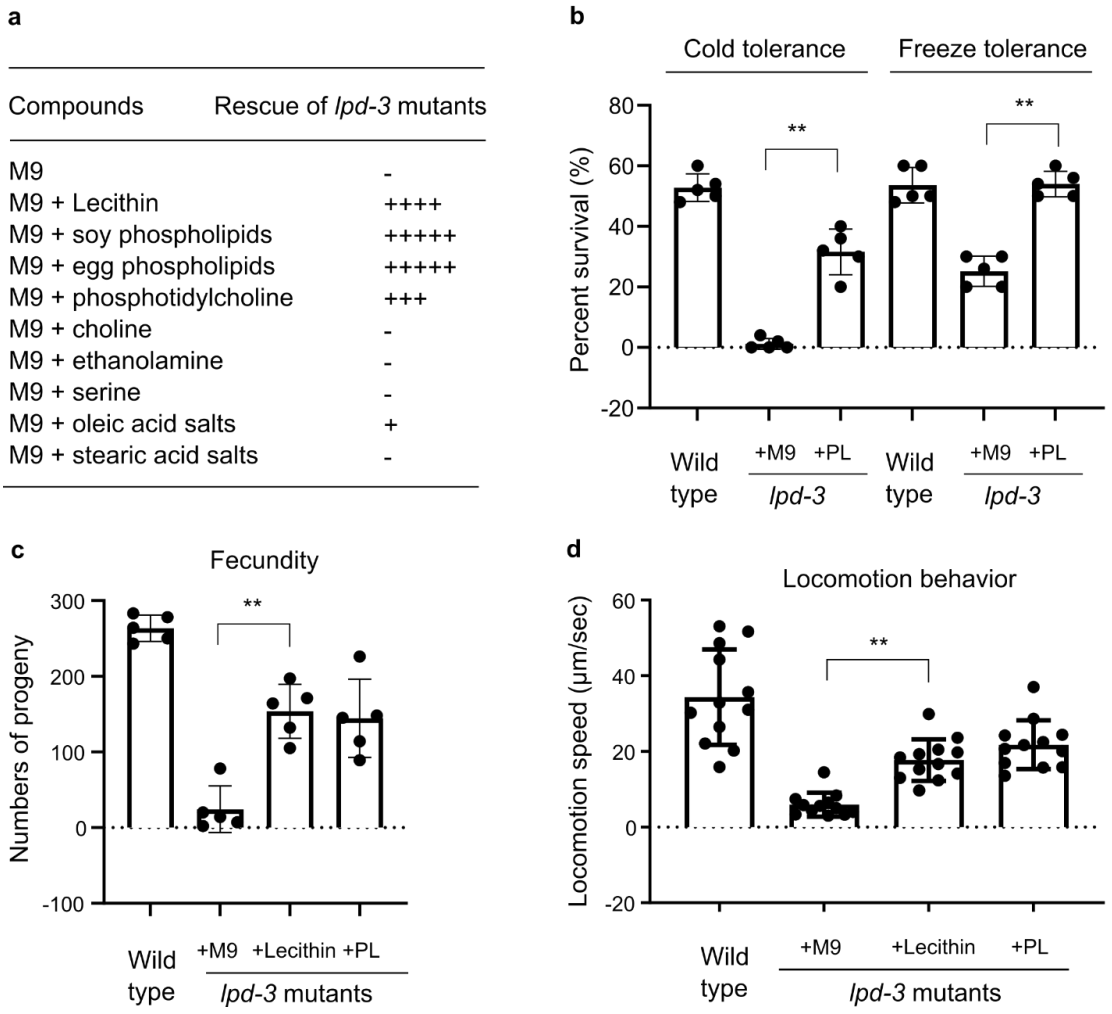

Extended Data Fig. 6. Phospholipid/Lecithin rescue of various *lpd-3* mutant phenotypes. a, Table summary for the degrees of rescue (indicated by the numbers of + sign) of developmental delay in *lpd-3* mutants by Lecithin, phospholipids derived from soy or egg, or various other phospholipid constituent compounds. **b**, Quantification of percent survival of wild type or *lpd-3* mutants, and rescue by soy phospholipid (PL), in the cold or freezing tolerance assays. Values are means ± S.D with $^{**}P < 0.01$ (N = 5 independent experiments, n > 50 animals for each experiment). **c**, Quantification of fecundity (numbers of progeny per hermaphrodite) of wild type or *lpd-3* mutants, and rescue by soy phospholipid (PL) or Lecithin. Values are means ± S.D with

583 $^{**}P < 0.01$ (n = 5 animals). **d**, Quantification of locomotion behavior (average speed of young

584 adult hermaphrodite) of wild type or *lpd-3* mutants, and rescue by soy phospholipid (PL) or

585 Lecithin. Values are means ± S.D with $^{**}P < 0.01$ (n = 10 animals for each condition).

586

Extended Data Figure 7

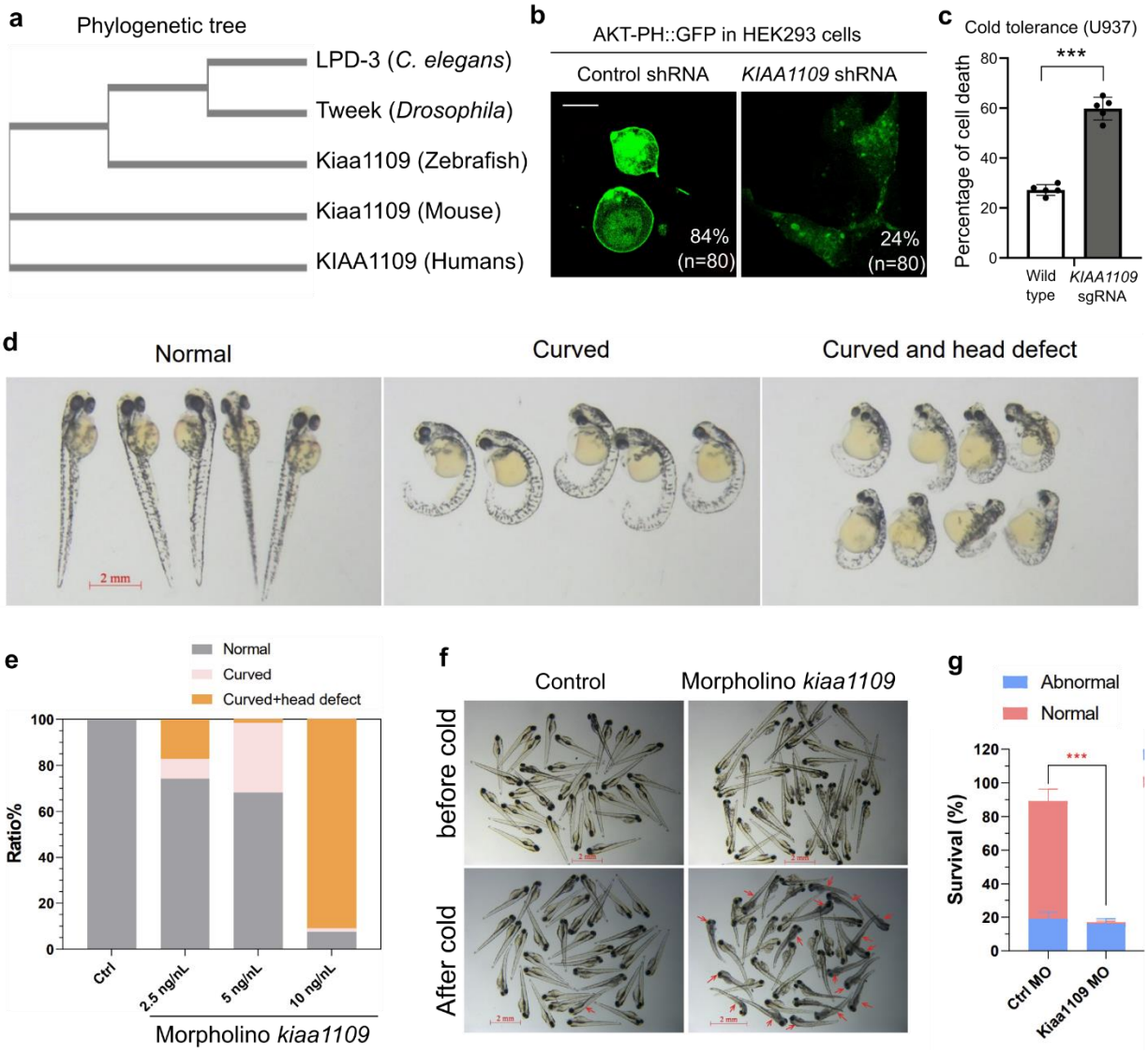

587

Extended Data Fig. 7. Evidence for conserved roles of LPD-3 protein families in lipid trafficking and cold tolerance. a, Clustal Omega-generated phylogenetic tree of the LPD-3 protein family from major metazoan species (*C. elegans*, *Drosophila*, Zebrafish, mouse and humans). **b**, Representative confocal fluorescence imaging of AKT-PH::GFP (PIP2/PIP3 binding) in HEK293 cells co-transfected with the AKT-PH::GFP and shRNA (control or *KIAA1109* with 73% knockdown efficiency, SIGMA) plasmids, showing reduced plasma membrane localization of AKT-PH::GFP by shRNA against *KIAA1109.* Percentages of cells with normal membrane-localized fluorescent signals were noted for shRNA control and sh-*KIAA1109*. **c**, Percentage of cell death after cold shock (4 ^{o}C for 20 hrs) in wild type and *KIAA1109* KO cells generated by CRISPR/Cas9. ***, $P < 0.001$; N = 5 independent experiments (n > 400 cells analyzed by SYTOX Green for each experiment). **d**, Representative images of zebrafish embryos showing various morphological phenotypes caused by morpholino against *kiaa1109*. **e**, Quantification of the various morphological phenotypes caused by morpholino against *kiaa1109*. **f**, Representative images of zebrafish embryos showing a phenotype of reduced cell survival caused by morpholino against *kiaa1109*. **g**, Quantification of reduced cell survival caused by morpholino against *kiaa1109.* Values are means ± S.D with ***, $P < 0.001$; N = 6 independent experiments (n > 30 fish for each experiment).

References

1. Ernst, R., Ejsing, C. S. & Antonny, B. Homeoviscous Adaptation and the Regulation of Membrane Lipids. *J. Mol. Biol.* **428**, 4776–4791 (2016).
2. de Mendoza, D. Temperature sensing by membranes. *Annu. Rev. Microbiol.* **68**, 101–116 (2014).

610 3. Ma, D. K. *et al.* Acyl-CoA Dehydrogenase Drives Heat Adaptation by Sequestering Fatty Acids. *Cell*
611 **161**, 1152–1163 (2015).
612 4. Lee, D. *et al.* MDT-15/MED15 permits longevity at low temperature via enhancing lipidostasis and
613 proteostasis. *PLoS Biol.* **17**, e3000415 (2019).
614 5. Bodhicharla, R., Devkota, R., Ruiz, M. & Pilon, M. Membrane Fluidity Is Regulated Cell
615 Nonautonomously by Caenorhabditis elegans PAQR-2 and Its Mammalian Homolog AdipoR2.
616 *Genetics* **210**, 189–201 (2018).
617 6. Devkota, R. *et al.* The adiponectin receptor AdipoR2 and its Caenorhabditis elegans homolog PAQR-2
618 prevent membrane rigidification by exogenous saturated fatty acids. *PLoS Genet.* **13**, e1007004
619 (2017).
620 7. Reinisch, K. M. & Prinz, W. A. Mechanisms of nonvesicular lipid transport. *J. Cell Biol.* **220**,
621 e202012058 (2021).
622 8. Vance, J. E. Phospholipid synthesis and transport in mammalian cells. *Traffic Cph. Den.* **16**, 1–18
623 (2015).
624 9. Kaplan, M. R. & Simoni, R. D. Intracellular transport of phosphatidylcholine to the plasma membrane.
625 *J. Cell Biol.* **101**, 441–445 (1985).
626 10. Sleight, R. G. & Pagano, R. E. Rapid appearance of newly synthesized phosphatidylethanolamine
627 at the plasma membrane. *J. Biol. Chem.* **258**, 9050–9058 (1983).
628 11. Kumar, N. *et al.* VPS13A and VPS13C are lipid transport proteins differentially localized at ER
629 contact sites. *J. Cell Biol.* **217**, 3625–3639 (2018).
630 12. Leonzino, M., Reinisch, K. M. & De Camilli, P. Insights into VPS13 properties and function reveal
631 a new mechanism of eukaryotic lipid transport. *Biochim. Biophys. Acta Mol. Cell Biol. Lipids* **1866**,
632 159003 (2021).

13. Melia, T. J. & Reinisch, K. M. A possible role for VPS13-family proteins in bulk lipid transfer, membrane expansion and organelle biogenesis. *J. Cell Sci.* **135**, jcs259357 (2022).

14. Toulmay, A. *et al.* Vps13-like proteins provide phosphatidylethanolamine for GPI anchor synthesis in the ER. *J. Cell Biol.* **221**, e202111095 (2022).

15. Adlakha, J., Hong, Z., Li, P. & Reinisch, K. M. Structural and biochemical insights into lipid transport by VPS13 proteins. *J. Cell Biol.* **221**, e202202030 (2022).

16. Neuman, S. D., Levine, T. P. & Bashirullah, A. A novel superfamily of bridge-like lipid transfer proteins. *Trends Cell Biol.* S0962-8924(22)00083–6 (2022) doi:10.1016/j.tcb.2022.03.011.

17. Kane, M. S. *et al.* Endosomal trafficking defects in patient cells with KIAA1109 biallelic variants. *Genes Dis.* **6**, 56–67 (2019).

18. Gueneau, L. *et al.* KIAA1109 Variants Are Associated with a Severe Disorder of Brain Development and Arthrogryposis. *Am. J. Hum. Genet.* **102**, 116–132 (2018).

19. Meszarosova, A. U. *et al.* Two novel pathogenic variants in KIAA1109 causing Alkuraya-Kučinskas syndrome in two Czech Roma brothers. *Clin. Dysmorphol.* **29**, 197–201 (2020).

20. Alazami, A. M. *et al.* Accelerating novel candidate gene discovery in neurogenetic disorders via whole-exome sequencing of prescreened multiplex consanguineous families. *Cell Rep.* **10**, 148–161 (2015).

21. Walker, A. K. *et al.* A conserved SREBP-1/phosphatidylcholine feedback circuit regulates lipogenesis in metazoans. *Cell* **147**, 840–852 (2011).

22. Li, Y., Na, K., Lee, H.-J., Lee, E.-Y. & Paik, Y.-K. Contribution of sams-1 and pmt-1 to lipid homoeostasis in adult Caenorhabditis elegans. *J. Biochem. (Tokyo)* **149**, 529–538 (2011).

23. Wu, G. & Vance, D. E. Choline kinase and its function. *Biochem. Cell Biol. Biochim. Biol. Cell.* **88**, 559–564 (2010).

656 24. Nomura, T., Horikawa, M., Shimamura, S., Hashimoto, T. & Sakamoto, K. Fat accumulation in
657 Caenorhabditis elegans is mediated by SREBP homolog SBP-1. *Genes Nutr.* **5**, 17–27 (2010).
658 25. Yang, F. *et al.* An ARC/Mediator subunit required for SREBP control of cholesterol and lipid
659 homeostasis. *Nature* **442**, 700–704 (2006).
660 26. Taubert, S., Hansen, M., Van Gilst, M. R., Cooper, S. B. & Yamamoto, K. R. The Mediator subunit
661 MDT-15 confers metabolic adaptation to ingested material. *PLoS Genet.* **4**, e1000021 (2008).
662 27. Brock, T. J., Browse, J. & Watts, J. L. Genetic regulation of unsaturated fatty acid composition in
663 C. elegans. *PLoS Genet.* **2**, e108 (2006).
664 28. Jiang, W. *et al.* A genetic program mediates cold-warming response and promotes stress-
665 induced phenoptosis in C. elegans. *eLife* **7**, (2018).
666 29. Yang, W., Dierking, K. & Schulenburg, H. WormExp: a web-based application for a
667 Caenorhabditis elegans-specific gene expression enrichment analysis. *Bioinforma. Oxf. Engl.* **32**, 943–
668 945 (2016).
669 30. Ding, W. *et al.* s-Adenosylmethionine Levels Govern Innate Immunity through Distinct
670 Methylation-Dependent Pathways. *Cell Metab.* **22**, 633–645 (2015).
671 31. Ashrafi, K. *et al.* Genome-wide RNAi analysis of Caenorhabditis elegans fat regulatory genes.
672 *Nature* **421**, 268–272 (2003).
673 32. Fraser, A. G. *et al.* Functional genomic analysis of C. elegans chromosome I by systematic RNA
674 interference. *Nature* **408**, 325–330 (2000).
675 33. McKay, R. M., McKay, J. P., Avery, L. & Graff, J. M. C elegans: a model for exploring the genetics
676 of fat storage. *Dev. Cell* **4**, 131–142 (2003).
677 34. Zhang, P. *et al.* Proteomic study and marker protein identification of Caenorhabditis elegans
678 lipid droplets. *Mol. Cell. Proteomics MCP* **11**, 317–328 (2012).

679 35. Mejia-Martinez, F. *et al.* The MXL-3/SBP-1 Axis Is Responsible for Glucose-Dependent Fat
680 Accumulation in C. elegans. *Genes* **8**, E307 (2017).
681 36. Shi, X. *et al.* Regulation of lipid droplet size and phospholipid composition by stearoyl-CoA
682 desaturase. *J. Lipid Res.* **54**, 2504–2514 (2013).
683 37. Jumper, J. *et al.* Highly accurate protein structure prediction with AlphaFold. *Nature* **596**, 583–
684 589 (2021).
685 38. Heo, W. D. *et al.* PI(3,4,5)P3 and PI(4,5)P2 Lipids Target Proteins with Polybasic Clusters to the
686 Plasma Membrane. *Science* **314**, 1458–1461 (2006).
687 39. Shi, A. *et al.* RAB-10-GTPase-mediated regulation of endosomal phosphatidylinositol-4,5-
688 bisphosphate. *Proc. Natl. Acad. Sci. U. S. A.* **109**, E2306-2315 (2012).
689 40. Sun, J., Harion, R., Naito, T. & Saheki, Y. INPP5K and Atlastin-1 maintain the nonuniform
690 distribution of ER-plasma membrane contacts in neurons. *Life Sci. Alliance* **4**, e202101092 (2021).
691 41. Quon, E. *et al.* Endoplasmic reticulum-plasma membrane contact sites integrate sterol and
692 phospholipid regulation. *PLoS Biol.* **16**, e2003864 (2018).
693 42. Gallo, A., Vannier, C. & Galli, T. Endoplasmic Reticulum-Plasma Membrane
694 Associations:Structures and Functions. *Annu. Rev. Cell Dev. Biol.* **32**, 279–301 (2016).
695 43. Henne, W. M., Liou, J. & Emr, S. D. Molecular mechanisms of inter-organelle ER-PM contact
696 sites. *Curr. Opin. Cell Biol.* **35**, 123–130 (2015).
697 44. Szumowski, S. C. *et al.* Small GTPases promote actin coat formation on microsporidian
698 pathogens traversing the apical membrane of Caenorhabditis elegans intestinal cells. *Cell. Microbiol.*
699 **18**, 30–45 (2016).
700 45. Hou, N. S. *et al.* Activation of the endoplasmic reticulum unfolded protein response by lipid
701 disequilibrium without disturbed proteostasis in vivo. *Proc. Natl. Acad. Sci. U. S. A.* **111**, E2271–E2280
702 (2014).

703 46. Rera, M., Clark, R. I. & Walker, D. W. Intestinal barrier dysfunction links metabolic and
704 inflammatory markers of aging to death in Drosophila. *Proc. Natl. Acad. Sci. U. S. A.* **109**, 21528–
705 21533 (2012).
706 47. Devkota, R. *et al.* A genetic titration of membrane composition in Caenorhabditis elegans
707 reveals its importance for multiple cellular and physiological traits. *Genetics* **219**, iyab093 (2021).
708 48. Liu, Y. & Lin, W. KIAA1109 is required for survival and for normal development and function of
709 the neuromuscular junction in mice. 2022.02.23.481678 Preprint at
710 https://doi.org/10.1101/2022.02.23.481678 (2022).
711 49. Jao, C. Y., Roth, M., Welti, R. & Salic, A. Metabolic labeling and direct imaging of choline
712 phospholipids in vivo. *Proc. Natl. Acad. Sci. U. S. A.* **106**, 15332–15337 (2009).
713 50. Ren, J. *et al.* Characterization of Biological Pathways Regulating Acute Cold Resistance of
714 Zebrafish. *Int. J. Mol. Sci.* **22**, 3028 (2021).
715 51. Sohlenkamp, C. & Geiger, O. Bacterial membrane lipids: diversity in structures and pathways.
716 *FEMS Microbiol. Rev.* **40**, 133–159 (2016).
717 52. John Peter, A. T. *et al.* Rewiring phospholipid biosynthesis reveals resilience to membrane
718 perturbations and uncovers regulators of lipid homeostasis. *EMBO J.* e109998 (2022)
719 doi:10.15252/embj.2021109998.
720 53. Verstreken, P. *et al.* Tweek, an evolutionarily conserved protein, is required for synaptic vesicle
721 recycling. *Neuron* **63**, 203–215 (2009).
722 54. Liu, Y. & Lin, W. Genetic deletion of Kiaa1109 in mice leads to developmental defects at the
723 neuromuscular junction. 2022.02.23.481678 Preprint at https://doi.org/10.1101/2022.02.23.481678
724 (2022).
725 55. Jeng, E. E. *et al.* Systematic Identification of Host Cell Regulators of Legionella pneumophila
726 Pathogenesis Using a Genome-wide CRISPR Screen. *Cell Host Microbe* **26**, 551-563.e6 (2019).

727 56. Brenner, S. The genetics of Caenorhabditis elegans. *Genetics* **77**, 71–94 (1974).

728 57. Davis, M. W. *et al.* Rapid single nucleotide polymorphism mapping in C. elegans. *BMC Genomics*
729 **6**, 118 (2005).

730 58. Ma, D. K., Vozdek, R., Bhatla, N. & Horvitz, H. R. CYSL-1 interacts with the O2-sensing
731 hydroxylase EGL-9 to promote H2S-modulated hypoxia-induced behavioral plasticity in C. elegans.
732 *Neuron* **73**, 925–940 (2012).

733 59. Kamath, R. S. & Ahringer, J. Genome-wide RNAi screening in Caenorhabditis elegans. *Methods*
734 *San Diego Calif* **30**, 313–321 (2003).

735 60. Mello, C. C., Kramer, J. M., Stinchcomb, D. & Ambros, V. Efficient gene transfer in C.elegans:
736 extrachromosomal maintenance and integration of transforming sequences. *EMBO J.* **10**, 3959–3970
737 (1991).

738 61. Pettersen, E. F. *et al.* UCSF Chimera--a visualization system for exploratory research and analysis.
739 *J. Comput. Chem.* **25**, 1605–1612 (2004).

740 62. Emsley, P. & Cowtan, K. Coot: model-building tools for molecular graphics. *Acta Crystallogr. D*
741 *Biol. Crystallogr.* **60**, 2126–2132 (2004).

742 63. Pettersen, E. F. *et al.* UCSF ChimeraX: Structure visualization for researchers, educators, and
743 developers. *Protein Sci. Publ. Protein Soc.* **30**, 70–82 (2021).

744 64. Kim, D., Langmead, B. & Salzberg, S. L. HISAT: a fast spliced aligner with low memory
745 requirements. *Nat. Methods* **12**, 357–360 (2015).

746 65. Love, M. I., Huber, W. & Anders, S. Moderated estimation of fold change and dispersion for
747 RNA-seq data with DESeq2. *Genome Biol.* **15**, 550 (2014).

748 66. Vozdek, R., Long, Y. & Ma, D. K. The receptor tyrosine kinase HIR-1 coordinates HIF-independent
749 responses to hypoxia and extracellular matrix injury. *Sci. Signal.* **11**, (2018).

750